Symmetry Propagation in Surface Supported Supramolecular Architectures of Terpyridines and Helicenes

Inauguraldissertation

Zur

Erlangung der Würde eines Doktors der Philosophie

vorgelegt der

Philosophisch-Naturwissenschaftlichen Fakultät

der Universität Basel

von

Thomas Nijs

aus Kaiseraugst (AG) und Belgien

Basel, 2018

Genehmigt von der Philosophisch-Naturwissenschaftlichen

Fakultät auf Antrag von:

Prof. Dr. Thomas Jung

Prof Dr. Catherine E. Housecroft

Basel, 19.09.2017

Prof. Dr. Martin Spiess
Dekan

"I think there is a world market for maybe five computers."

Thomas Watson, president of IBM, 1943

"God made the bulk; the surface was invented by the devil."

Wolfgang Pauli

Publication list

During my PhD studies, I have contributed to the following publications (chronological order). Four further manuscripts are currently in-progress, five more upcoming in near future.

[1] Phase transitions in confinements: Controlling solid to Fluid transitions of xenon atoms in an on-surface network DOI: 10.1002/smll.201803169, *Small* (2018)

[2] The different faces of 4'-pyrimidinyl functionalized 4,2':6',4"-terpyridines: metal organic assemblies from solution and on Au(111) and Cu(111) surface platforms
DOI: 10.1021/jacs.7b12624, *Journal of the American Chemical Society*, 140 (2018)

[3] Adsorbate-induced modification of the confining barriers in a quantum box array
DOI: 10.1021/acsnano.7b07989, *ACS Nano*, 12 (2017)

[4] Long-range ferrimagnetic order in a two-dimensional supramolecular Kondo lattice
DOI: 10.1038/ncomms1538, *Nature Communications*, 8 (2017)

[5] Molecular chessboard assemblies sorted by site-specific interactions of out-of-plane d-orbitals with a semimetal template
DOI: 10.1021/acs.nanolett.6b05344, *Nano letters*, 17 (2017)

[6] Configuring Electronic States in an Atomically Precise Array of Quantum Boxes
DOI: 10.1002/smll.201600915, *Small*, 12 (2016)

[7] Programmed assembly of 4,2':6',4"-terpyridine derivatives into porous, on-surface networks
DOI: 10.1039/C5CC04186D, *Chemical Communications*, 51 (2015)

[8] Interplay of weak interactions in the atom-by-atom condensation of xenon within quantum boxes DOI: 10.1038/ncomms7071, *Nature Communications*, 6 (2015)

[9] Controlling the Dimensionality of On-Surface Coordination Polymers via Endo- or Exoligation DOI: 10.1021/ja5020103, *Journal of the American Chemical Society*, 136 (2014)

[10] Chirality Transfer in 1D Self-Assemblies: Influence of H-Bonding vs Metal Coordination between Dicyano[7]helicene Enantiomers
DOI: 10.1021/ja407315f, *Journal of the American Chemical Society*, 135 (2013)

Table of Contents

Abstract

The tunability of molecular self-assemblies together with the principles of supramolecular chemistry are the base of this thesis. In order to gain deeper insight into bigger bottom-up complexes like 3D metal organic frameworks (MOFs) or 2D hierarchical assemblies, we break down their dimensionality and complexity and monitor the on-surface self-organization behavior of the individual molecules.

In chapter [[1]] we introduce first on-surface results of a newly designed 4,2':6',4''-terpyridine. Its shape is specially designed to allow in-plane assemblies, in contrast to the 'standard' chelating 2,2':6',2''-terpyridines. We present nanoporous networks for both hydrogen bonded and metal coordinated assemblies, investigate their change in bonding and their adaptability to the surface reconstruction due to changed substrate interactions.

In chapter [[2]] we extend this study and try to answer the question how far can we scale up these simplified 2D investigations into the 3D world? Thereby we make use of an unique concept, by directly comparing the very same compounds in both cases: we compare the 2D self-organization in vacuum environment on Au(111) and Cu(111) surfaces and the role of Cu-adatoms with its in-solution counterparts comprising different Cu-salts and its resulting x-ray crystals. Beside this, due to utilization of different molecular functionalizations and external applied parameters, we further demonstrate the strength and tunability of such networks, and the influences even the smallest changes in the building block can exhibit on the large scale.

In chapter [[3]] we present another example of growth, namely 2D hierarchical with propagation of chirality. We investigate the chirality transfer from a single molecule over a hydrogen bonded trimer to an extended supramolecular assembly upon coordination. The latter is comprised of a trimeric structure of cobalt coordinated trimers hold together by weaker van der Waals forces. In this examination we employ both, enantiopure and racemic mixtures.

Abbreviations and molecules

0D	zero dimensional
1D	one dimensional
2D	two dimensional
3D	three dimensional
BE	binding energy
LDOS	local density of states
MOF	metal organic framework
MON	metal organic network
n	nano = 10^{-9}
STM	scanning tunneling microscopy scanning tunneling microscope
STS	scanning tunneling spectroscopy
tpy	terpyridine
UHV	ultra high vacuum
vdW	van der Waals
XPS	x-ray photoelectron spectroscopy

Molecules / Chemical compounds:

Top view Side view

DiOH[6]Hel 2,3-dihydroxy[6]helicene

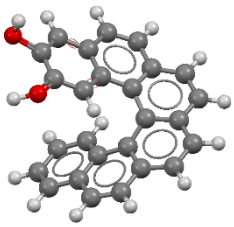

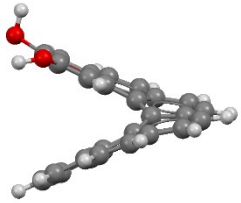

4'-imidazole-4,2':6',4"-terpyridine

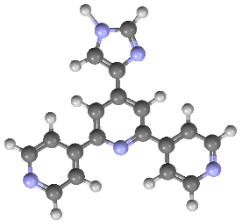

4'-(pyrimidin-5-yl)-4,2':6',4"-terpyridine

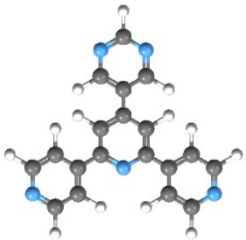

4'-(2-methylpyrimidin-5-yl)-4,2':6',4"-terpyridine

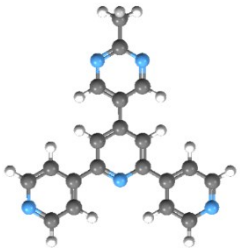

4'-(2-ethylpyrimidin-5-yl)-4,2':6',4"-terpyridine

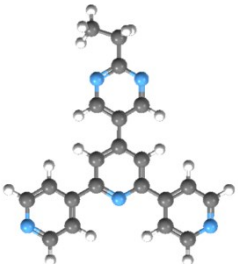

Introduction

The process of miniaturization is unstoppable. Already it has reached all aspects of our daily lives. Applications seem endless, advantages obvious.[1] One of the most prominent examples of this process are electronic devices, benefiting by becoming more compact and versatile (key word: ubiquitous computing), yet less power consuming, less heat producing and more powerful. Electronics are also for another reason a hot topic currently in the world of miniaturization: it is predicted that classic physical limits are going to be reached soon beyond which new technologies will be needed.[2] Already now Moore's law[3] is overtaking again, after manufacturing had been slightly ahead of it (please see IEEE Spectrum for more background information[4-5]) and with the current so-called 10 nm technology node chip production* the popular top-down fabrication approach can only be continued for the next 2-3 chipset generations (as the minimal distance is set at 2-3 nm, equivalent to around ten single atoms, before quantum mechanical problems will occur like tunneling currents[6]).

As stated in a recent article from the World Economic Forum,[7] we as nanoscientists might overcome this problem by changing the approach from top-down to bottom-up, focusing for example on single molecular self-assemblies. This allows for an easy way of entering the quantum world, since due to the well-defined interplay of guiding attractive and repulsive forces during the self-assembly, when repeated under same conditions, this approach allows for consistent manufacturing in a fast and economical way of structures consisting of single molecules or eventually atoms.[8]

Being in the field of research, we are trying to find the perfect parameters which lead to stable and reproducible self-assemblies. So far, this still happens predominantly by simple screening experiments. In other disciplines such as pharmacy this is a common practice eg. for testing of drugs by using microtiter plates.[9] These screening tests have been developed to such extend, also with the help of miniaturization, that several thousands of different targets can be tested in one go, and at the example of microfluidic chips with only the need of a few nL of sample each.[10] As since also the readout is optimized and automatized, this is a perfectly acceptable method. For our purposes however, this is not suitable. A method is desired that allows to predict

* Formerly equivalent to half pitch distance between DRAM elements (Dynamic Random Access Memory). Nowadays name mainly used for marketing reasons.

the outcome of especially bigger bottom-up assemblies comprised from individual building-units at chosen parameters. This would allow for a preselection of the experiments to be made, and in a potentially future step to completely skip the "trial and error" experiments.

Inspiration was found in biochemistry and crystallography, both regarding folding mechanisms of proteins: the sequence-to-structure (-to-function) paradigm.[11] As mentioned earlier, DNA sequence readout runs at an incredible speed at present. Next step would be to derive the structure of a protein (eg. alpha helixes and beta sheets and their corresponding tertiary and quaternary structures) and in a future step the function based on the shape, all by simple readout of the DNA base sequence. We are chasing the same dream with molecules, to make a prediction from the single building blocks, employed in known, fixed parameters, to predict the self-assembly of multi-dimensional assemblies, based on the rules of supramolecular chemistry and bonding geometry.

In summary, an idea originating from *biochemistry* is employed for predicting *chemical* forces based on mainly *physical* investigation methods, exploring single molecule building blocks and atomic interactions. This is the true concept of Nanoscience.

This thesis presents a first example of a direct comparison of the same compounds at the solid-vacuum interphase vs. in-solution. The ultimate goal is to assemble a toolkit database, allowing for better understanding of complex bottom-up multi-dimensional assemblies (dimension can also be equivalent to 'property'). One of the ideas was for instance to 'look' inside of a 3D MOF by analyzing its 2D self-assembly, thereby simplifying the investigation by direct real-space access.

Methods

The main investigation techniques used for this work can be separated in 2 groups: real-space structural characterization complemented by spectroscopic measurements. The first is performed by scanning tunneling microscopy (STM), the second by X-ray photoelectron spectroscopy (XPS).

STM:

Due to its process of data acquisition, scanning tunneling microscopy measurements allow for both, convoluted topographical and electronical depiction of the molecules on the (conductive metallic) sample, in real space. It makes use of the non-classical tunneling current, a current flowing (tunneling) through a barrier height >> than the energy of the electrons along the bias applied between measurement tip and sample. This tunneling regime however only lasts in a very small tip-sample distance (couple of Angströms), apparent by solving the Schrödinger equation. This exposes the exponential decay of the tunneling current vs. distance, making it very topography dependent. At the same time however, the local density of states (LDOS) is also reflected in the signal by the fact of having – at a specific energy (tunable by applied voltage bias) – regions where electrons can be easier extracted (or collected) than others. This accessibility of electrons, is dependent on material and will alter the signal strength.

XPS:

Illuminating a sample with electromagnetic radiation releases photoelectrons. The model behind this effect (photoelectric effect) secured Einstein the Nobel Prize in 1921. Analyzing the energy of those released electrons gives direct relation to the orbital (meaning the chemical element) they originate from, since $E_{\text{binding}} = E_{\text{radiation}} - E_{\text{electron}}$ (E_{rad} is known from source and E_{el} by detector, E_{bind} is the element specific electron extraction energy). Small changes in this binding energy reflect changes in the local environment of the electrons such we cannot only discriminate between the different elements, but we also get an idea in which state they are due to the so-called chemical shift. In addition to this qualitative measurement, also stoichiometry can be analyzed by counting the events of a specific energy hitting the detector.

Results

This thesis is based on the following first-author publications and is provided in the 'cumulative' format. The publications and manuscripts are listed below and are referred in the text by double square brackets:

[[1]] Programmed assembly of 4,2':6',4"-terpyridine derivatives into porous, on-surface networks / DOI: 10.1039/C5CC04186D, *Chemical Communications*, 51 (2015)

[[2]] The different faces of 4'-pyrimidinyl functionalized 4,2':6',4"-terpyridines: metal organic assemblies from solution and on Au(111) and Cu(111) surface platforms
DOI: 10.1021/jacs.7b12624, *Journal of the American Chemical Society*, 140 (2018)

[[3]] Hierarchical chirality transfer of DiOH[6]Hel on the self-assembly pattern: interplay of the complex intermolecular bonding / T. Nijs et al.

Chapter [[1]]

Programmed assembly of 4,2':6',4''-terpyridine derivatives into porous, on-surface networks
DOI: 10.1039/C5CC04186D, *Chemical Communications*, 51 (2015)

Summary:

This research focuses on the bonding motif change of imidazole functionalized terpyridine molecules upon Cu-adatom addition on Au(111) surface. Two co-existent hydrogen bonded phases (close-packed and nanoporous) recombine into differently sized metal coordinated macrocycles. Chains of these macrocycles are trapped inside the herringbone surface reconstruction, resulting in overproportional appearance of 5 membered rings, as a compromise between the angle optimized 6 membered and the space optimized 4 membered ones.

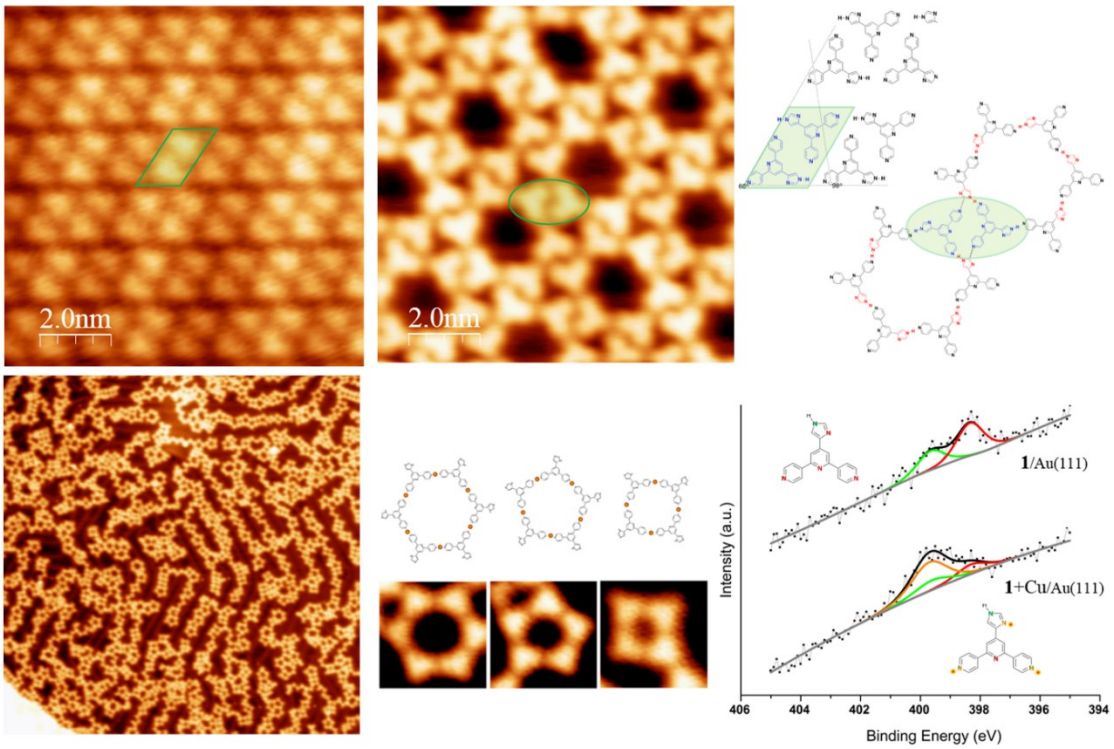

Contribution of T. Nijs: carried out the experimental investigation (STM, XPS), analysed and interpreted the data, wrote the manuscript; all with the help of F. J. Malzner.

ChemComm

COMMUNICATION

View Article Online
View Journal | View Issue

Programmed assembly of 4,2′:6′,4″-terpyridine derivatives into porous, on-surface networks†

Thomas Nijs,[a] Frederik J. Malzner,[b] Shadi Fatayer,[ac] Aneliia Wäckerlin,[a] Sylwia Nowakowska,[a] Edwin C. Constable,[b] Catherine E. Housecroft*[b] and Thomas A. Jung*[d]

Cite this: *Chem. Commun.*, 2015, **51**, 12297

Received 21st May 2015,
Accepted 23rd June 2015

DOI: 10.1039/c5cc04186d

www.rsc.org/chemcomm

The use of divergent, V-shaped, 4,2′:6′,4″-terpyridine building blocks that self-assemble into hydrogen-bonded domains and upon addition of copper atoms undergo metallation with concomitant transformation into a coordination network is described; multiple energetically similar structural motifs are observed in both hydrogen-bonded and adatom-coordinated networks.

The assembly of 2-dimensional metal–organic networks on surfaces is topical[1] in view of their relationship to 3-dimensional metal–organic frameworks (MOFs).[2] However, the mechanism of their assembly (co-determined by the proximity of the surfaces and the presence of adatoms) remains sparsely investigated. Examples of systems which exhibit on-surface association through hydrogen bonding or metal coordination using well defined and controllable motifs include 4,9-diaminoperylene-quinone-3,10-diimine, helicenes and porphyrins.[3–8]

In contrast to the chelating ligand 2,2′:6′,2″-terpyridine (2,2′:6′,2″-tpy),[9] 4,2′:6′,4″-terpyridine (4,2′:6′,4″-tpy) coordinates through only two N atoms and defines a divergent V-shaped building-block allowing control over the assembly of coordination polymers and networks.[10] Part of the attractiveness of 4,2′:6′,4″-tpy ligands in supramolecular chemistry is the simplicity of the synthetic routes[11] to 4′-aryl functionalized derivatives (Scheme 1) which allows facile structural and electronic tuning. On-surface investigations of terpyridines are limited. Scanning tunnelling microscopy (STM) shows that 2,2′:6′,2″-tpy solution-cast onto Au(111) adsorbs with molecules oriented orthogonally to the surface with dominant intermolecular π-stacking.[12]

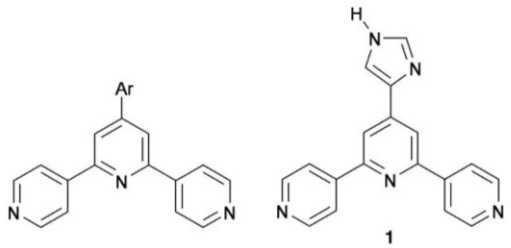

Scheme 1 General 4′-aryl-functionalized 4,2′:6′,4″-terpyridine and the imidazole-functionalized ligand **1**.

A variety of STM studies of adsorbed functionalized 2,2′:6′,2″-tpys, of adsorbed $[M(2,2':6',2''\text{-tpy})_2]^{n+}$ complexes, and of metal coordination-driven assemblies on either highly ordered pyrolytic graphite (HOPG), Pt(111), Au(111) or Cu(100) have been reported,[13] and a recent publication reveals the influence that solvent has in directing surface assemblies from drop-cast films of 1,16-bis([2,2′:6′,2″-terpyridin]-4′-yloxy)hexadecane.[14] However, on-surface assemblies of 4,2′:6′,4″-terpyridines and their metal complexes remain unexplored.

We present here an investigation of the imidazolyl-functionalized derivative **1** (Scheme 1) on Au(111) and the effects of the addition of copper adatoms. We have previously reported the solid-state structure of **1** $CHCl_3$ and showed that $NH_{imidazole}\cdots N_{tpy}$ hydrogen bonds are favoured over $NH_{imidazole}\cdots N_{imidazole}$ interactions, consistent with the relative basicities of the heterocycles.[15] The solid-state structure of only one complex of **1** has been described; in $[\{2Co(\mathbf{1})_2(NCS)_2\cdot 5H_2O\}_n]$, the imidazole domain and the central N atom of the 4,2′:6′,4″-tpy unit are not coordinated.[15] A feature of **1** relevant to on-surface assembly is the fact that it is prochiral.

After deposition on an Au(111) substrate, **1** self-assembles into a close-packed phase (Fig. 1b and c) which co-exists with a regular 6-fold nanoporous structure (Fig. 1d and e); between the two phases lies a domain with an irregular assembly pattern (Fig. 1a). The two phases can be rationalized in terms of different intermolecular hydrogen-bonding patterns. The co-existence of two phases is reproducible in different samples

[a] *Department of Physics, University of Basel, Klingelbergstrasse 82, 4056 Basel, Switzerland*
[b] *Department of Chemistry, University of Basel, Spitalstrasse 51, 4056 Basel, Switzerland. E-mail: catherine.housecroft@unibas.ch*
[c] *Instituto de Física "Gleb Wataghin", Universidade Estadual de Campinas, Rua Sérgio Buarque de Holanda 777, 13083-859 Campinas, SP, Brazil*
[d] *Laboratory for Micro- and Nanotechnology, Paul Scherrer Institut, 5232 Villigen, Switzerland. E-mail: thomas.jung@psi.ch*

† Electronic supplementary information (ESI) available: Additional Fig. S1–S5; Tables S1 and S2 with XPS data. See DOI: 10.1039/c5cc04186d

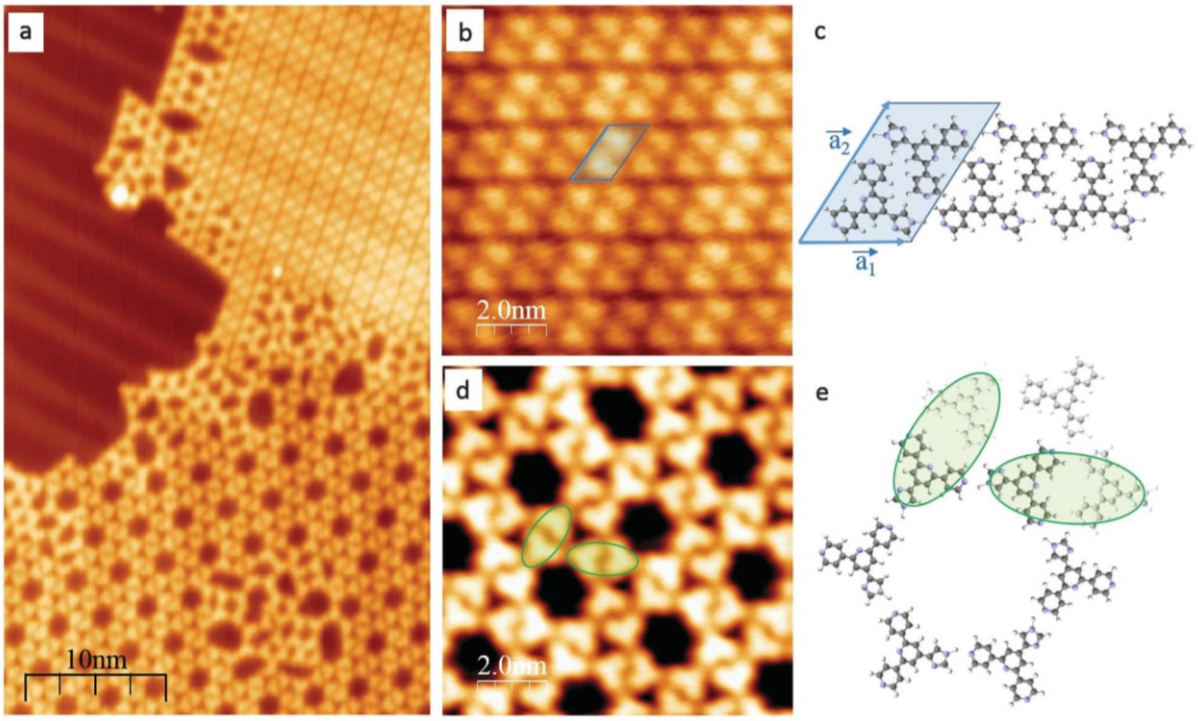

Fig. 1 STM images of hydrogen bonded structures of **1** on Au(111). (a) STM image of two coexisting phases: on top, a close-packed array, at the bottom a network structure. Note the irregular assemblies where the two phases meet. (b) STM image of the close-packed phase composed of molecular rows that consists of dimers shown in (c). (c) Model for the adsorption of molecules presents a rhombic shape with lattice constants equal to a_1 = (1.21 ± 0.06) nm, a_2 = (1.95 ± 0.06) nm and α = (56 ± 2)°. (d) STM image of the hexagonal porous network. The distance between pores of the network is (3.09 ± 0.03)nm and the diameter of the pores is (1.38 ± 0.06) nm which gives an area of (1.52 ± 0.08) nm^2. (e) Model of a pore in the network with three adjacent molecules (see d); two dimer motifs are highlighted to illustrate part of a chiral 'flower' pattern that runs around the macrocycle.

and is consistent with a small energy difference between the 2-dimensional assembly motifs.

The first compact assembly (Fig. 1b) consists of a hydrogen-bonded linear double row arrangement, each of these separated by a small gap, due to resulting repulsive interactions (Fig. S1†). The principal motif in the porous assembly is a hexameric array. This is well-modelled by molecules of **1** engaging in $NH_{imidazole}\cdots N_{tpy}$ hydrogen bonding and forming a chiral motif (Fig. 1e and Fig. S2†). All the hexamers in the domain possess the same handedness and the relationship between adjacent cyclic motifs can be seen by defining the dimer shown in Fig. 1e and Fig. S2.† Domains with opposite handedness are present on the surface (Fig. S3†). The hydrogen-bonded supramolecular arrangement of **1** is not significantly influenced by the atomic lattice of the underlying substrate which bears the $Au(111)(22 \times \sqrt{3})$ reconstruction.[16] The weak corrugation of the supramolecular layer can be attributed to the stacking fault zones of that same reconstruction, visible in both the close-packed and nanoporous phases, and possesses comparable periodicity. This observation of coexisting compact and porous 2-dimensional assemblies is not unique, and of particular relevance are results from Reichert *et al.*[6] who have described a prochiral carbonitrile derivative assembling on Ag(111) in coexisting dense and enantiopure porous phases. The assembly shown in Fig. 1d is similar to a Kagome lattice;[17,18] the latter comprises a regular network of interconnected hexagons and triangles, whereas in Fig. 1d, closer association of the hexagonal motifs leads to a reduction in the triangular domains.

After sublimation of Cu onto the hydrogen-bonded assemblies of **1** on Au(111), the supramolecular adlayer changes its structure. Chains of linked heterocyclic macrocycles, which generally follow the fcc domains of the $Au(111)(22 \times \sqrt{3})$ reconstruction, are clearly observed by STM (Fig. 2a). These mostly form regular polygons. The transition upon adding Cu adatoms from extended networks with pseudo-hexagonal symmetry showing little distortion by the Au(111) surface reconstruction, to the oligomeric structures with a preference for the fcc domains of the reconstructed surface, suggests a modified substrate–adsorbate interaction. Such behaviour is plausible for molecular modules coordinated *via* metal adatoms which are in registry with the substrate atoms. In addition to the STM topographs recorded at 5 K, the local chemical transitions were also analysed by X-ray Photoelectron Spectroscopy (XPS) measurements. These confirm metal coordination by investigating the N 1s binding energies of **1** (Fig. 2b and Table S1†). Prior to coordination, two peaks are observed; the higher energy peak corresponds to $NH_{imidazole}$ (399.6 eV, green in Fig. 2b) and the lower to –N= (398.3 eV, red in Fig. 2b, both tpy and imidazole) with a well-fitting energy difference of 1.3 eV.[19,20] Instead of the ratio being 1 : 4 corresponding to the structure of **1**, it is closer to 2 : 3. This could be due to surface charge effects and/or intermolecular

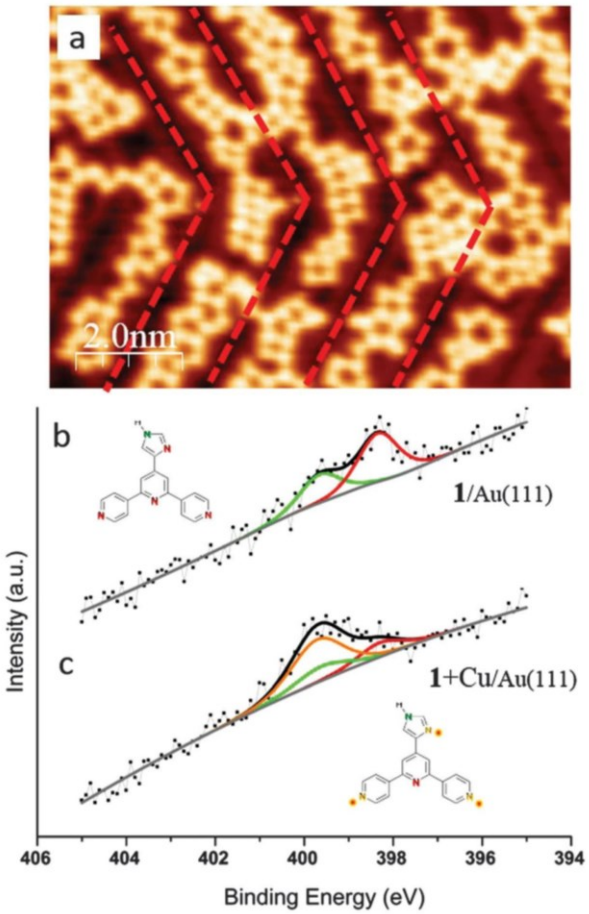

Fig. 2 Metal coordination of **1** on Au(111). (a) STM image shows the metal coordinated structures, which are oriented along the fcc region of the Au(111) herringbone reconstruction (highlighted in red; see also Fig. S4†). (b and c) XPS spectra showing the N environment of **1** before (b) and after (c) deposition of copper adatoms. The peak deconvolution reveals two uncoordinated species (the central N_{tpy} and $NH_{imidazole}$, red and green respectively), whereas the remaining N energy shift upwards consistent with coordination.

hydrogen bonds,[21] as the multilayer shows 1 : 4 stoichiometry with corresponding peak positions of 400.3 eV respectively 398.9 eV (Fig. S5†). As stated earlier, $NH_{imidazole}$ and the central N_{tpy} of **1** remain uncoordinated upon Cu-adatom addition and this is consistent with the XPS peaks shown in green and red in Fig. 2b which remain at the same peak positions (Fig. 2b *versus* Fig. 2c). The second $N_{imidazole}$ and the two outer pyridine N_{tpy} undergo coordination which is confirmed by a shift of 1.4 eV to higher binding energy to 399.7 eV (orange in Fig. 2c).[22] The ratio of peak areas (orange : green : red in Fig. 2c) was set to be 2 : 1 : 1. The binding energies for uncoordinated and coordinated molecules are summarized in Table S1.†

The presence of various sized and shaped macrocycles (Fig. 3a) is consistent with (i) metal-binding through only the outer N-donors of the 4,2′:6′,4″-tpy unit (as confirmed crystallographically for 4,2′:6′,4″-tpy complexes[10]) and (ii) a balance between molecule–molecule and increased molecule–substrate interactions. The internal angle of the divergent 4,2′:6′,4″-tpy domain is 120° and ideally matched to a hexameric assembly. However, the histogram in Fig. 3b reveals that this 6-fold assembly appears only in a minority of on-surface motifs which comprise 3-, 4-, 5- and 6-membered macrocycles, indicating the presence of an additional limiting factor beyond the macrocycle ring strain. This can be attributed to the width of the fcc region of the herringbone reconstruction, limiting the area of the macrocycles.[23] The 6-membered macrocycle represents the most favourable angle configuration, the 4-membered the most favourable size configuration, and the presence of the 5-membered macrocycles represents a compromise of both cases. In each of the 4-, 5- and 6-membered metallomacrocycles, coordination involving only the 4,2′:6′,4″-tpy domain is proposed. However, this coordination mode would lead to a strained 3-membered cyclic array. Comparison of the four images in Fig. 3a clearly reveals that the larger rings have 6-, 5- and 4-fold symmetry, whereas the trimer appears 'squashed' and is not 3-fold symmetric; furthermore, 3-membered rings are only observed as motifs on the periphery of larger rings. Metal binding involving both N_{tpy} and $N_{imidazole}$ is consistent with these observations (Fig. 3a, right). Other examples are known, where the Au(111) herringbone reconstruction guides the molecular assembly. The fcc and hcp differ not only in topography, but also possess different electronic properties (the hcp stacked top layer is more electron rich).[24] Therefore, molecules have preferential adsorption sites,[25] especially if there is a strong interaction with the substrate (*e.g. via* dipolar interactions[26] or *via* metal coordination[4]).

In conclusion, we have shown that **1** assembles on a Au(111) surface into a close-packed phase which co-exists with a 6-fold nanoporous structure. The prochirality of **1** results in each hexacycle possessing a handedness and the chirality persists throughout the domain, with domains of both chiralities being present. Best-fit models are consistent with $NH_{imidazole}\cdots N_{tpy}$ hydrogen bonds being the dominant interactions. The introduction of

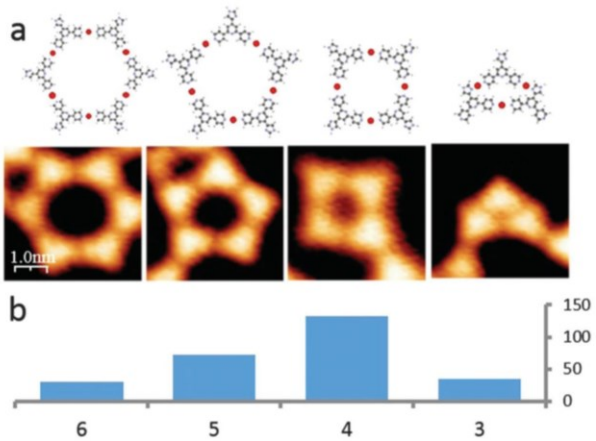

Fig. 3 Macrocycle distribution. (a) Models and respective STM images of the most appearing macrocycles. (b) Histogram reveals existence of preferential pore-geometry, which are macrocycles consisting out of 3, 4, 5 or 6 molecular building blocks.

copper adatoms switches the on-surface assembly to discrete cyclic structures, the size distribution of which is consistent with the Au(111) herringbone reconstruction guiding the molecular assembly.

We thank the Swiss Nano Institute, Swiss National Science Foundation (Grant 200020_149067), São Paulo Research Foundation FAPESP (Grant 2013/04855-0) and the University of Basel for support. Marco Martina is thanked for supporting the infrastructure and co-developing and maintaining the sample preparation and handling procedures; a prototype of a vacuum suitcase (KTI PSPM and Ferrovac Inc) has been used in this work. Srboljub Vujovic is thanked for supplying ligand **1**.

References

1 C. A. Palma, M. Cecchini and P. Samori, *Chem. Soc. Rev.*, 2012, **41**, 3713; J. V. Barth, *Surf. Sci.*, 2009, **603**, 1533.
2 F. Bebensee, K. Svane, C. Bombis, F. Masini, S. Klyatskaya, F. Besenbacher, M. Ruben, B. Hammer and T. R. Linderoth, *Angew. Chem., Int. Ed.*, 2014, **53**, 12955 and references cited therein.
3 M. Matena, J. Björk, M. Wahl, T.-L. Lee, J. Zegenhagen, L. H. Gade, T. A. Jung, M. Persson and M. Stöhr, *Phys. Rev. B: Condens. Matter Mater. Phys.*, 2014, **90**, 235419.
4 A. Shchyrba, M.-T. Nguyen, C. Wäckerlin, S. Martens, S. Nowakowska, T. Ivas, J. Roose, T. Nijs, S. Boz, M. Schär, M. Stöhr, C. A. Pignedoli, C. Thilgen, F. Diederich, D. Passerone and T. A. Jung, *J. Am. Chem. Soc.*, 2013, **135**, 15270.
5 S. L. Tait, Y. Wang, G. Costantini, N. Lin, A. Baraldi, F. Esch, L. Petaccia, S. Lizzit and K. Kern, *J. Am. Chem. Soc.*, 2008, **130**, 2108.
6 J. Reichert, M. Marschall, K. Seufert, D. Ecija, W. Auwärter, E. Arras, S. Klyatskaya, M. Ruben and J. V. Barth, *J. Phys. Chem. C*, 2013, **117**, 12858.
7 See for example: Y. Li, J. Xiao, T. E. Shubina, M. Chen, Z. Shi, M. Schmid, H.-P. Steinrück, J. M. Gottfried and N. Lin, *J. Am. Chem. Soc.*, 2012, **134**, 6401; T. Lin, Q. Wu, J. Liu, Z. Shi, P. N. Liu and N. Lin, *J. Chem. Phys.*, 2015, **142**, 101909; G. Lyu, R. Zhang, X. Zhang, P. N. Liu and N. Lin, *J. Mater. Chem. C*, 2015, **3**, 3252.
8 See for example: J. I. Urgel, D. Ecija, W. Auwärter, D. Stassen, D. Bonifazi and J. V. Barth, *Angew. Chem., Int. Ed.*, 2015, **54**, 6163; S. Vijayaraghavan, D. Ecija, W. Auwärter, S. Joshi, K. Seufert, M. Drach, D. Nieckarz, P. Szabelski, C. Aurisicchio, D. Bonifazi and J. V. Barth, *Chem. – Eur. J.*, 2013, **19**, 14143; D. Heim, D. Écija, K. Seufert, W. Auwärter, C. Aurisicchio, C. Fabbro, D. Bonifazi and J. V. Barth, *J. Am. Chem. Soc.*, 2010, **132**, 6783.
9 E. C. Constable, *Chem. Soc. Rev.*, 2007, **36**, 246; E. C. Constable, *Chimia*, 2013, **67**, 388 and references cited therein.
10 C. E. Housecroft, *Dalton Trans.*, 2014, **43**, 6594.
11 J. Wang and G. S. Hanan, *Synlett*, 2005, 1251.
12 L. S. Pinheiro and M. L. A. Temperini, *Surf. Sci.*, 2000, **464**, 176.
13 See for example: P. R. Andres, R. Lunkwitz, G. R. Pabst, K. Böhn, D. Wouters, S. Schmatloch and U. S. Schubert, *Eur. J. Org. Chem.*, 2003, 3769; D. J. Díaz, S. Bernhard, G. D. Storrier and H. D. Abruña, *J. Phys. Chem. B*, 2001, **105**, 8746; C. Grave, D. Lentz, A. Schäfer, P. Samori, J. P. Rabe, R. Franke and A. D. Schlüter, *J. Am. Chem. Soc.*, 2003, **125**, 6907; E. C. Constable, H.-J. Güntherodt, C. E. Housecroft, L. Merz, M. Neuburger, S. Schaffner and Y. Tao, *New J. Chem.*, 2006, **20**, 1470; T. Albrecht, K. Moth-Poulsen, J. B. Christensen, A. Guckian, T. Bjørnholm, J. G. Vos and J. Ulstrup, *Faraday Discuss.*, 2006, **131**, 265; E. Figgemeier, L. Merz, B. A. Hermann, Y. C. Zimmermann, C. E. Housecroft, H.-J. Guntherodt and E. C. Constable, *J. Phys. Chem. B*, 2003, **107**, 1157; W. Wang, S. Wang, Y. Hong, B. Z. Tang and N. Lin, *Chem. Commun.*, 2011, **47**, 10073; X. Q. Shi, W. H. Wang, S. Y. Wang, N. Lin and M. A. Van Hove, *Catal. Today*, 2011, **177**, 50; D. Trawny, P. Schlexer, K. Steenbergen, J. P. Rabe, B. Paulus and H.-U. Reissig, *ChemPhysChem*, 2015, **16**, 949; S. L. Tait, A. Langner, N. Lin, S. Stepanow, C. Rajadural, M. Ruben and K. Kern, *J. Phys. Chem. C*, 2007, **111**, 10982.
14 S. Wang, F. Zhao, S. Luo, Y. Geng, Q. Zeng and C. Wang, *Phys. Chem. Chem. Phys.*, 2015, **17**, 12350.
15 E. C. Constable, C. E. Housecroft, M. Neuburger, S. Vujovic, J. A. Zampese and G. Zhang, *CrystEngComm*, 2012, **14**, 3554.
16 J. V. Barth, H. Brune, G. Ertl and R. J. Behm, *Phys. Rev. B: Condens. Matter Mater. Phys.*, 1990, **42**, 9307 and references therein.
17 Z. Shi and N. Lin, *J. Am. Chem. Soc.*, 2009, **131**, 5376.
18 F. Klappenberger, D. Kühne, W. Krenner, I. Silanes, A. Arnau, F. J. García de Abajo, S. Klyatskaya, M. Ruben and J. V. Barth, *Nano Lett.*, 2009, **9**, 3509.
19 J. S. Stevens, A. C. de Luca, M. Pelendritis, G. Terenghi, S. Downes and S. L. M. Schroeder, *Surf. Interface Anal.*, 2013, **45**, 1238.
20 J. M. L. Martínez, E. Rodríguez-Castellón, R. M. Torres Sánchez, L. R. Denaday, G. Y. Buldain and V. Campo Dall' Orto, *J. Mol. Catal.*, 2011, **339**, 43.
21 A. Shchyrba, C. Wäckerlin, J. Nowakowski, S. Nowakowska, J. Björk, S. Fatayer, J. Girovsky, T. Nijs, S. C. Martens, A. Kleibert, M. Stöhr, N. Ballav, T. A. Jung and L. H. Gade, *J. Am. Chem. Soc.*, 2014, **136**, 9355.
22 C. H.-H. Traulsen, E. Darlatt, S. Richter, J. Poppenberg, S. Hoof, W. E. S. Unger and C. A. Schalley, *Langmuir*, 2012, **28**, 10755; D. Skomski, C. D. Tempas, K. A. Smith and S. L. Tait, *J. Am. Chem. Soc.*, 2014, **136**, 9862.
23 L.-A. Fendt, M. Stöhr, N. Wintjes, M. Enache, T. A. Jung and F. Diederich, *Chem. – Eur. J.*, 2009, **15**, 11139.
24 W. Chen, V. Madhavan, T. Jamneala and M. Crommie, *Phys. Rev. Lett.*, 1998, **80**, 1469.
25 M. E. Cañas-Ventura, K. Aït-Mansour, P. Ruffieux, R. Rieger, K. Müllen, H. Brune and R. Fasel, *ACS Nano*, 2011, **5**, 457; Y. Pan, B. Yang, C. Hulot, S. Blechert, N. Nilius and H.-J. Freund, *Phys. Chem. Chem. Phys.*, 2012, **14**, 10987; I. Fernandez-Torrente, S. Monturet, K. J. Franke, J. Fraxedas, N. Lorente and J. I. Pascual, *Phys. Rev. Lett.*, 2007, **99**, 176103; M. Yu, N. Kalashnyk, R. Barattin, Y. Benjalal, M. Hliwa, X. Bouju, A. Gourdon, C. Joachim, E. Lægsgaard, F. Besenbacher and T. R. Linderoth, *Chem. Commun.*, 2010, **46**, 5545.
26 M. Böhringer, K. Morgenstern, W.-D. Schneider, M. Wühn, C. Wöll and R. Berndt, *Surf. Sci.*, 2000, **444**, 199.

Electronic Supplementary Material (ESI) for ChemComm.

ESI to accompany:

Programmed assembly of 4,2':6',4''-terpyridine derivatives into porous, on-surface networks

Thomas Nijs, Frederik J. Malzner, Shadi Fatayer, Aneliia Wäckerlin, Sylwia Nowakowska, Edwin C. Constable, Catherine E. Housecroft* and Thomas A. Jung*

Methods section

Samples were prepared and investigated under ultrahigh vacuum (UHV) conditions with a base pressure of 5×10^{-11} mbar. Substrates were prepared by cycles of sputtering the Au(111) crystal (MaTecK GmbH) with Ar^+ ions at 1 keV and subsequent annealing at 630 K. Molecule deposition onto the sample was done by thermal evaporation from a commercial evaporator (Kentax GbmH) at 480 K. Metal adatoms were supplied by e-beam evaporator (Oxford Applied Research). Coverage was controlled by a quartz crystal microbalance. All preparation steps and the X-ray photoelectron spectroscopy (XPS) measurements were carried out at room temperature. The XPS measurements were performed at the Laboratory for Micro- and Nano-technology at the Paul Scherrer Institute (PSI). A monochromatic Al kα X-ray source was used, resulting in a full width at half maximum (FWHM) of 1 eV. Peak analysis was performed with Unifit software. All STM images were recorded with 1 V and 10 pA, at 5 K in constant current mode (Omicron Nanotechnology GmbH) and processed with WSxM software.[1] The STM tip was made of 90% Pt and 10% Ir wire, mechanically cut and sputtered *in situ* with Ar^+ ions.

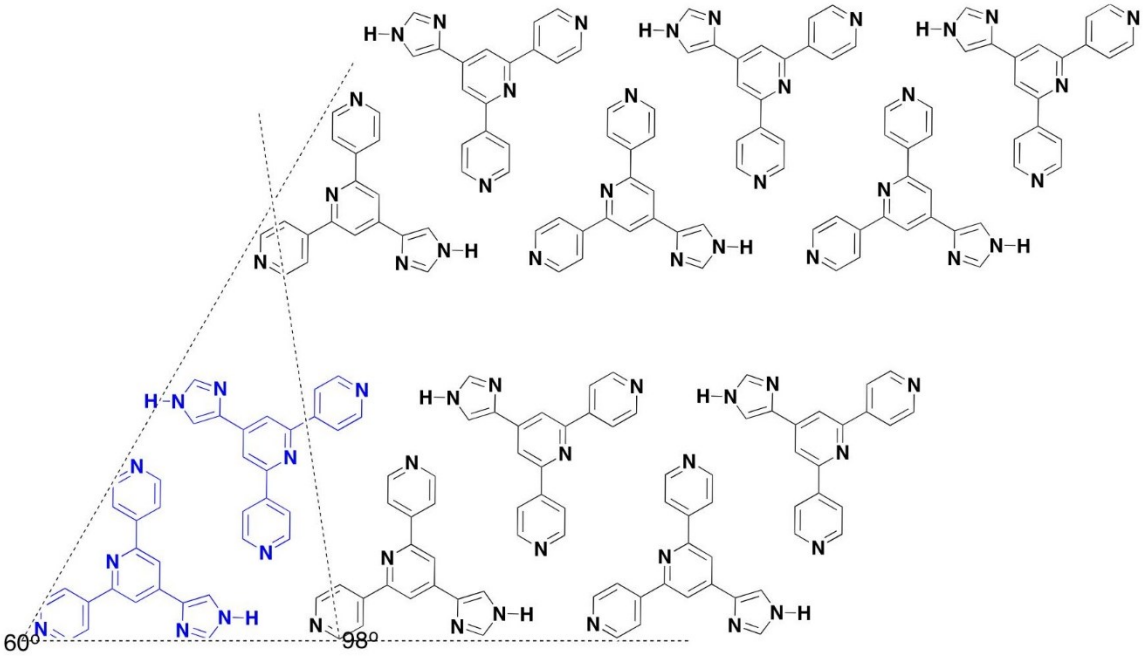

Fig. S1. Arrangement of molecules of **1** in the close-packed domain which permits $NH_{imidazole}\cdots N_{tpy}$ hydrogen bond formation.

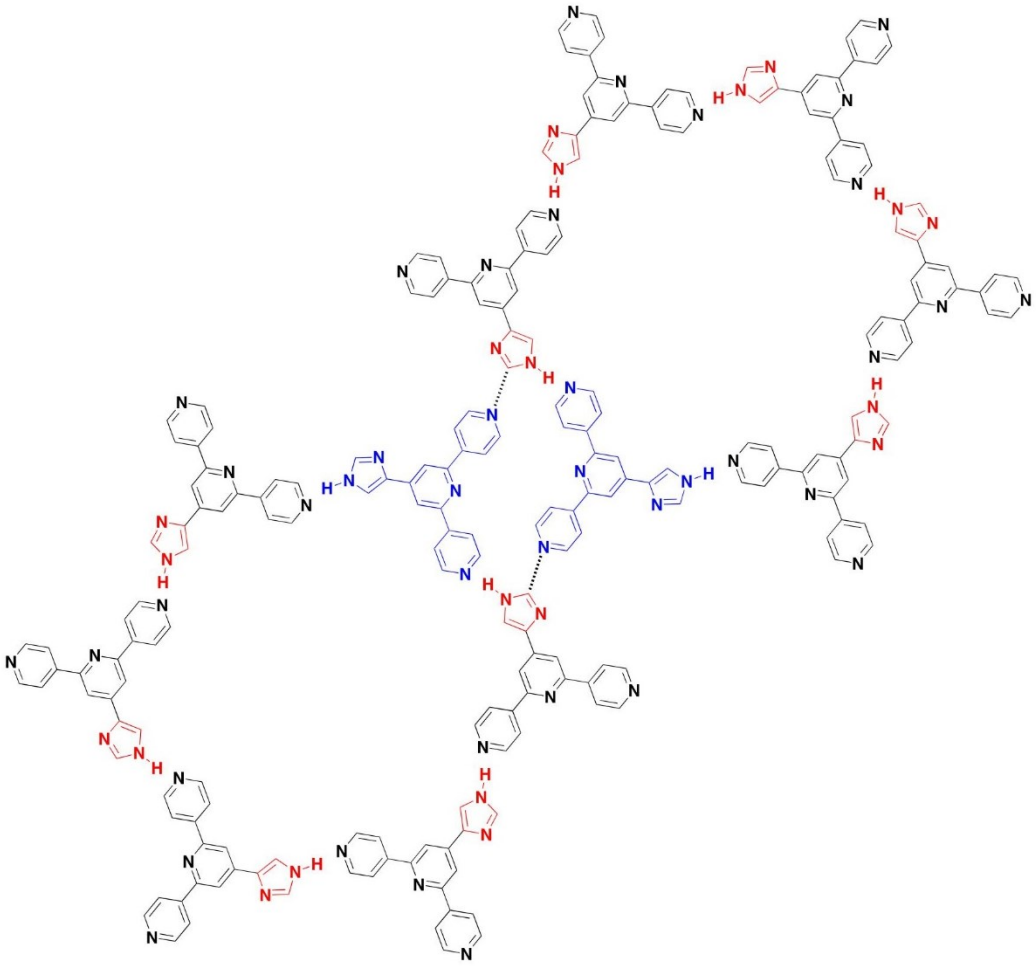

Fig. S2. Chirality imposed on the 6-fold motif supported by $NH_{imidazole}\cdots N_{tpy}$ hydrogen bonds (imidazole units in red); one dimeric motif between adjacent hexamers is highlighted in blue.

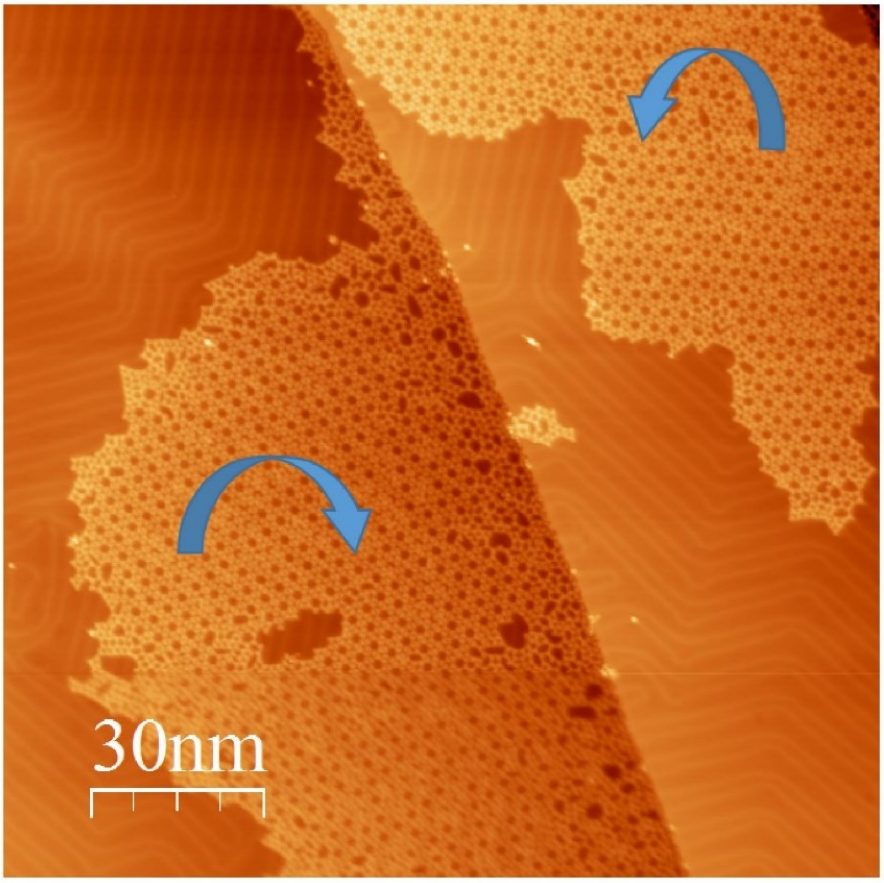

Fig. S3. Domains with opposite handedness are present on the Au(111) surface.

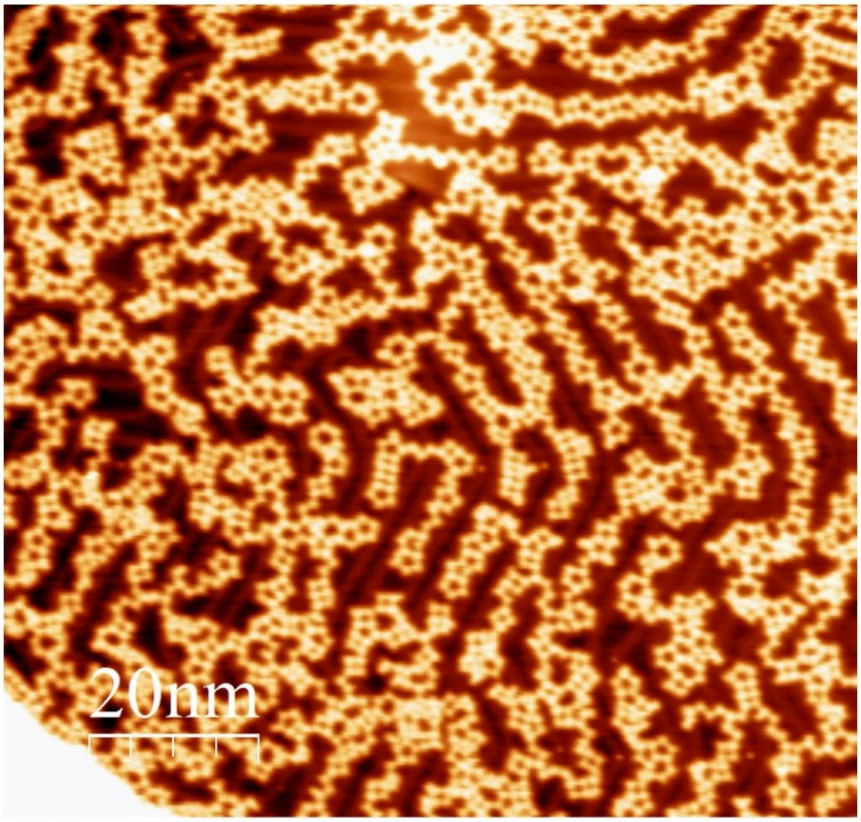

Fig. S4. Overview image showing the chains of metallomacrocycles which generally follow the Au(111) herringbone reconstruction.

5

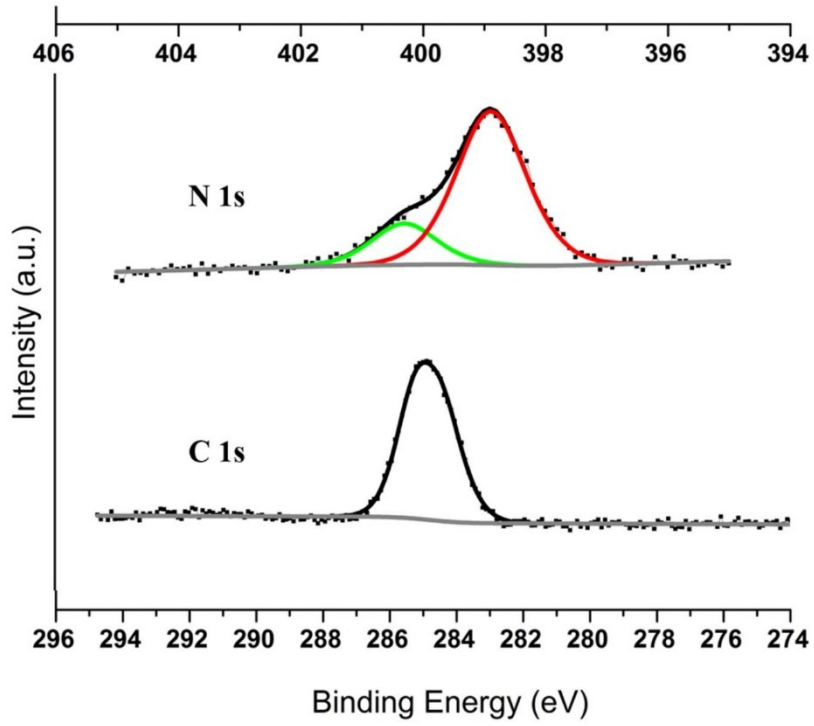

Fig. S5: XPS analysis of multilayers of **1** on Au(111).
Total C:N ratio => 3.6:1 (corresponding to 18:5)
N 1s deconvolution => -NH- : -N= ratio is 1:4
Detailed N 1s peak positions analysis is presented in Table S1.

Table S1: XPS N 1s peak positions of **1** experimentally obtained, imidazole –NH, pyridine and imidazole –N=, and Cu-coordinated N.

Molecule/Substrate	**-NH** [eV]	**-N=** [eV]	**N-Cu** [eV]
Multilayer **1**/Au(111)	400.3	398.9	-
1/Au(111)	399.6	398.3	-
1+Cu/Au(111)	399.6	398.3	399.7

Table S2: Literature comparison of values in Table S1.

-NH [eV]	**-N=** [eV]	**N-Cu** [eV]
399.9[2]	398.3[4]	400.2[4]
399.8[3]	398.6[2]	
	398.8[3]	

1 I. Horcas, R. Fernandez, J.M. Gomez-Rodriguez, J. Colchero, J. Gomez-Herrero and A. M. Baro, *Rev. Sci. Instru*m., 2007, **78**, 013705.
2 X. F. Dai, J. L. Qiao, X. J. Zhou, J. J. Shi, P. Xu, L. Zhang and J. J. Zhang, *Int. J. Electrochem. Sci*., 2013, **8**, 3160.
3 A. Shchyrba, C. Wäckerlin, J. Nowakowski, S. Nowakowska, J. Björk, S. Fatayer, J. Girovsky, T. Nijs, S. C. Martens, A. Kleibert, M. Stöhr, N. Ballav, T. A. Jung and L. H. Gade, *J. Am. Chem. Soc*., 2014, **136**, 9355.
4 D. Skomski, C. D. Tempas, K. A. Smith and S. L. Tait, *J. Am. Chem. Soc*., 2014, **136**, 9862.

Chapter [[2]]

The different faces of 4'-pyrimidinyl functionalized 4,2':6',4"-terpyridines: metal organic assemblies from solution and on Au(111) and Cu(111) surface platforms
DOI: 10.1021/jacs.7b12624, *Journal of the American Chemical Society*, 140 (2018)

Summary:

Three almost identical pyrimidine functionalized terpyridines molecules, only differing in R = 'H', 'methyl' or 'ethyl' residue, have been employed in both, on-surface and in-solution experiments allowing for direct comparison. On the surface of a Cu(111) substrate, we can follow up the in-situ multi-stage metal coordination change from a 2D close-packed assembly, over 1D chains, quasi 0D tetramers till a 2D coordinated network, only by annealing steps. Additionally, these assemblies depend on the smallest changes of the residue. In contrast, the in-solution self-assembly is mainly guided by the employed Cu-salt solution, and the way in which it links two neighboring molecules. Cu(II)-acetate allows for planar 2D sheet which are associated through π-stacking of the terpyridine cores, whereas for Cu(I)-triflate, the triflate anions drive inter-sheet hydrogen bonding.

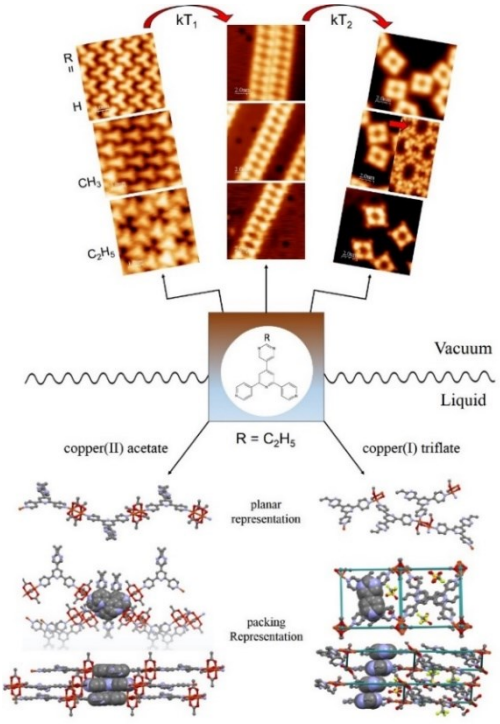

Contribution of T. Nijs: carried out the on-surface investigation (STM, XPS), analysed and interpreted the data, wrote the manuscript. In-solution contribution by Y. M. Klein.

JACS JOURNAL OF THE AMERICAN CHEMICAL SOCIETY
Article
Cite This: J. Am. Chem. Soc. 2018, 140, 2933−2939
pubs.acs.org/JACS

The Different Faces of 4′-Pyrimidinyl-Functionalized 4,2′:6′,4′′-Terpyridines: Metal−Organic Assemblies from Solution and on Au(111) and Cu(111) Surface Platforms

Thomas Nijs,[†] Y. Maximilian Klein,[‡] S. Fatemeh Mousavi,[†] Aisha Ahsan,[†] Sylwia Nowakowska,[†] Edwin C. Constable,[‡] Catherine E. Housecroft,*[,‡] and Thomas A. Jung*[,†,§]

[†]Department of Physics, University of Basel, Klingelbergstrasse 82, 4056 Basel, Switzerland
[‡]Department of Chemistry, University of Basel, BPR 1096, Mattenstrasse 24a 4058 Basel, Switzerland
[§]Laboratory for Micro- and Nanotechnology, Paul Scherrer Institut, 5232 Villigen, Switzerland

Supporting Information

ABSTRACT: A comparative investigation of crystal growth from solution and on-surface assembly *in vacuo* between copper and three 4′-(2-R-pyrimidin-5-yl)-4,2′:6′,4′′-terpyridines, with R = H (**1**), Me (**2**), or Et (**3**), is presented. In solution, ligand **3** combines with copper(II) acetate or copper(I) triflate in MeOH solution to give $[Cu_2(OAc)_4(\mathbf{3})]_n$ or $\{[Cu(\mathbf{3})(OMe)(MeOH)][CF_3SO_3]\cdot MeOH\}_n$. In $[Cu_2(OAc)_4(\mathbf{3})]_n$, paddle-wheel $\{Cu_2(\mu\text{-}OAc)_4\}$ nodes direct the assembly of one-dimensional (1D) zigzag chains which pack into two-dimensional (2D) sheets. In $\{[Cu(\mathbf{3})(OMe)(MeOH)][CF_3SO_3]\cdot MeOH\}_n$, the solvent is a ligand and also generates $\{Cu_2(\mu\text{-}OMe)_2\}$ units which function as planar 4-connecting nodes to generate a 2D (4,4) net with ligand **3**. On Au(111) or Cu(111) surfaces *in vacuo*, no additional solvent or anions are involved in the assembly. The different substituents in **1**, **2**, or **3** allow precise molecular resolution imaging in scanning tunneling microscopy. On Au(111), **1** and **2** assemble into close-packed assemblies, while **3** forms a regular porous network. The deposition of Cu adatoms results in reorganization leading to ladder-shaped surface metal−organic motifs. These on-surface coordination assemblies are independent of the 4′-substituent in the 4,2′:6′,4′′-tpy and are reproduced on Cu(111) where Cu adatoms are available during the deposition and relaxation process at room temperature. Upon annealing at elevated temperatures, the original surface assemblies of **1** and **3** are modified and a transition from ladders into rhomboid structures is observed; for **2**, a further quasi-hexagonal nanoporous network is observed.

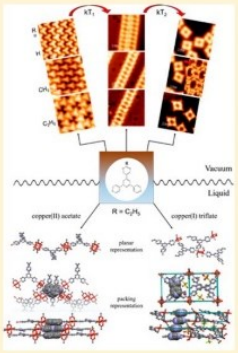

INTRODUCTION

One of the most common strategies for supramolecular assembly is predicated upon the interactions of metal centers with ligands.[1] Metallosupramolecular chemistry[2] is concerned with the matching of commensurate metal centers and metal-binding domains. In contrast to single carbon centers which typically exhibit one of three coordination geometries (two-coordinate linear, three-coordinate planar, and four-coordinate tetrahedral), metal centers can exhibit coordination numbers from one to at least 12 with all possible geometries.[3] Furthermore, the metal−ligand bond may be labile or kinetically inert, allowing access to a dynamic system.[1] These interactions may be used for the assembly of discrete supramolecular systems or extended one-, two-, or three-dimensional (1D, 2D, or 3D) assemblies collectively known as coordination polymers.[4] Metal−organic frameworks (MOFs) are well-established 3D examples with wide-ranging applications in catalysis, electrochemistry, host−guest chemistry, and fuel cells.[5] Two-dimensional networks can be assembled on an atomically flat substrate, allowing templated host−guest interactions in any pockets in the 2D lattice. Nevertheless, 3D and 2D assemblies differ in the elastic response of the host network and in 2D networks interaction with the substrate can mediate cooperative effects[6−8] We are interested in the multi-dimensional structural diversity which can be achieved through variation in molecular structure and processing in bulk materials and in monolayers. We also wish to probe the structural consequences of the constraints of assembly processes on-surfaces as opposed to those in solution.

Of the 48 isomers of terpyridine, the best known is 2,2′:6′,2′′-terpyridine (2,2′:6′,2′′-tpy, Chart 1) which is a chelating ligand typically presenting a convergent *N,N′,N′′*-donor set to a metal center,[9] whereas the less well-investigated 4,2′:6′,4′′-tpy and 3,2′:6′,3′′-tpy (Chart 1) only coordinate to metal centers through the terminal nitrogen donors and present divergent *N,N′*-donor sets ideal for the assembly of extended structures with metal nodes.[10,11] Functionality can readily be introduced at the 4′-position[12,13] allowing the construction of ligands with both innocent and non-innocent substituents. Although 4,2′:6′,4′′-tpy ligands are well-established in 1D and 2D systems,[9,11] few examples of 3D networks in the absence of peripheral coordination units or co-ligands have been described.[14,15]

In networks of 4,2′:6′,4′′-tpy ligands with copper nodes, anions or co-ligands play a critical role in directing the

Received: December 5, 2017
Published: February 9, 2018

DOI: 10.1021/jacs.7b12624
J. Am. Chem. Soc. 2018, 140, 2933−2939

Chart 1. Coordination Modes of Isomeric Terpyridines 2,2′:6′,2″-tpy, 3,2′:6′,3″-tpy, and 4,2′:6′,4″-tpy[a]

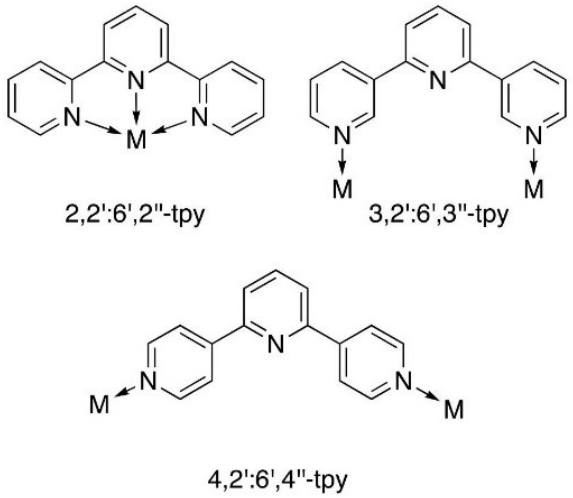

[a]The structural diversity possible with 3,2′:6′,3″-tpy is greater because of rotation about the interannular C−C bonds.

assembly. Reactions of CuCN with 4′-aryl-4,2′:6′,4″-tpy ligands lead to interpenetrated 3D frameworks with bridging 4,2′:6′,4″-tpy and cyanido ligands. Increasing the steric demands of the 4′-functionality suppresses the interpenetration.[16] Bridging cyanido linkers also feature in interpenetrated 3D frameworks found in $[Cu_9(4'\text{-}(NCC_6H_4)\text{-}4,2':6',4''\text{-}tpy)_{4.5}(CN)_9]_n$ (see Chart 2 for the structure of 4′-(NCC_6H_4)-4,2′:6′,4″-tpy).[17] In both of these networks, the copper(I) centers are 3-coordinate. A carboxylic acid group in the 4′-position of the tpy unit is typically non-innocent,[17−20] although Xiao and co-workers suggest that the presence of uncoordinated $-CO_2H$ moieties play a role in the assembly of an unusual 2D → 2D polythreaded network.[21] The ligand 4′-(4-pyridyl)-4,2′:6′,4″-tpy (Chart 2) is well-explored, and coordination to copper(I) through both the 4,2′:6′,4″-tpy and pendant pyridyl units leads to a 3D network with 4-fold interpenetration; in this case nitrate counterions and MeOH solvent molecules are accommodated along channels in the structure.[22] Reactions of copper(II) acetate with 4′-aryl-4,2′:6′,4″-tpy's (aryl = biphenylyl,[23] 2′,3′,4′,5′,6′-pentafluorobiphenyl,[23] phenyl,[24] 4-dimethylaminophenyl[24]) lead to 1D coordination polymers incorporating paddle-wheel $\{Cu_2(\mu\text{-}OAc)_4\}$ nodes connected by bridging 4,2′:6′,4″-tpy domains.

Chart 2. Structures of Selected 4′-Functionalized 4,2′:6′,4″-tpy Ligands

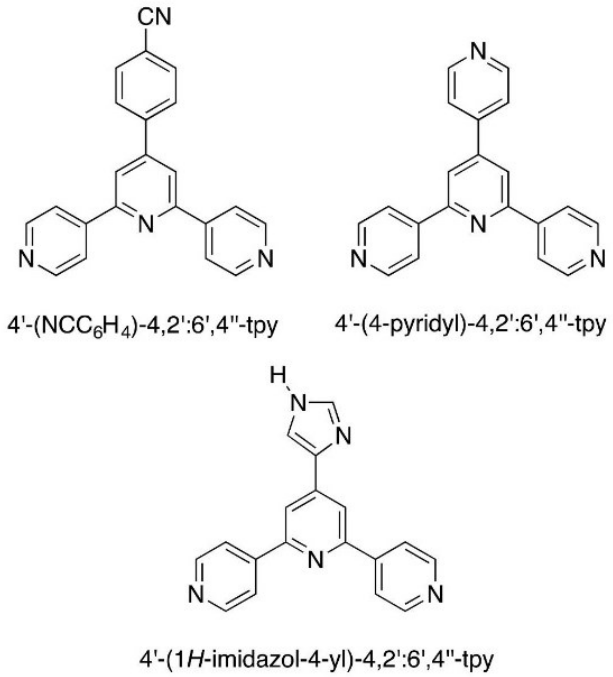

We are interested in 4,2′:6′,4″-tpy building blocks functionalized in the 4′-position with *N*-heterocycles other than pyridine, and focus upon copper as the metal node for the assembly of multi-dimensional networks. The originality of our approach is to combine studies of crystal growth under ambient solution conditions with on-surface deposition on Au(111) and Cu(111) substrates under ultrahigh vacuum (UHV) to investigate the interactions of these ligands with metal centers. This strategy allows us to probe the assembly process with a constant pairing of metal and ligand with and without constraints imposed by a surface architecture. In solution, the oxidation state of the metal-node (Cu^+ or Cu^{2+}) is defined *and* counterions are required for charge neutrality; furthermore, crystallization typically results in incorporation of lattice solvent molecules. In contrast, on-surface assemblies initiated by copper adatoms yield structures free from counterions and solvent molecules. Both 4′-(1*H*-imidazol-4-yl)-4,2′:6′,4″-tpy (Chart 2) and 4′-(pyrimidin-5-yl)-4,2′:6′,4″-tpy (**1**, Chart 3) are attractive building blocks containing both a divergent V-shaped tecton and a functionality with potential for further coordination although their coordination chemistry has been little explored. Each might direct the assembly of 1D chains or 2D networks depending upon the coordinative innocence or non-innocence of the pendant heterocyclic substituent. 4′-(1*H*-Imidazol-4-yl)-4,2′:6′,4″-tpy forms hydrogen-bonded domains on an Au(111) surface, and the addition of copper adatoms results in reorganization into a 2D coordination network; the *N*-donors of both the 4,2′:6′,4″-tpy and imidazolyl units are bonded to copper.[25] In the only example of a coordination assembly involving 4′-(1*H*-imidazol-4-yl)-4,2′:6′,4″-tpy under solution conditions, the imidazolyl unit is uncoordinated.[26] We have also shown that **1** and its 2-methyl-substituted derivative **2** bind zinc(II) selectively through the 4,2′:6′,4″-tpy domain.[27] In contrast, the pendant pyrimidinyl domains in $[Ru(\mathbf{4})_2]^{2+}$ (Chart 3) bind copper(II) to generate a 2D network.[28] In the present work, we report the coordination behavior of pyrimidinyl-functionalized ligands **1**−**3** (Chart 3) with copper with an emphasis on contrasting the coordination behavior in solution with on-surface interactions of these ligands with copper adatoms. The surface-immobilized networks can be tuned by varying the length of any 2-substituent attached to the pyrimidine ring or through external stimulus in the form of annealing.

■ EXPERIMENTAL SECTION

Experimental details and crystallographic data are given in the Supporting Information.

■ RESULTS AND DISCUSSION

Synthesis and Characterization of Compound 3. We have previously reported ligands **1** and **2**,[27] and compound **3**

DOI: 10.1021/jacs.7b12624
J. Am. Chem. Soc. 2018, 140, 2933−2939

Chart 3. Structures of Ligands 1−3 and of the Pyrimidyl-Functionalized Complex $[Ru(4)]^{2+}$

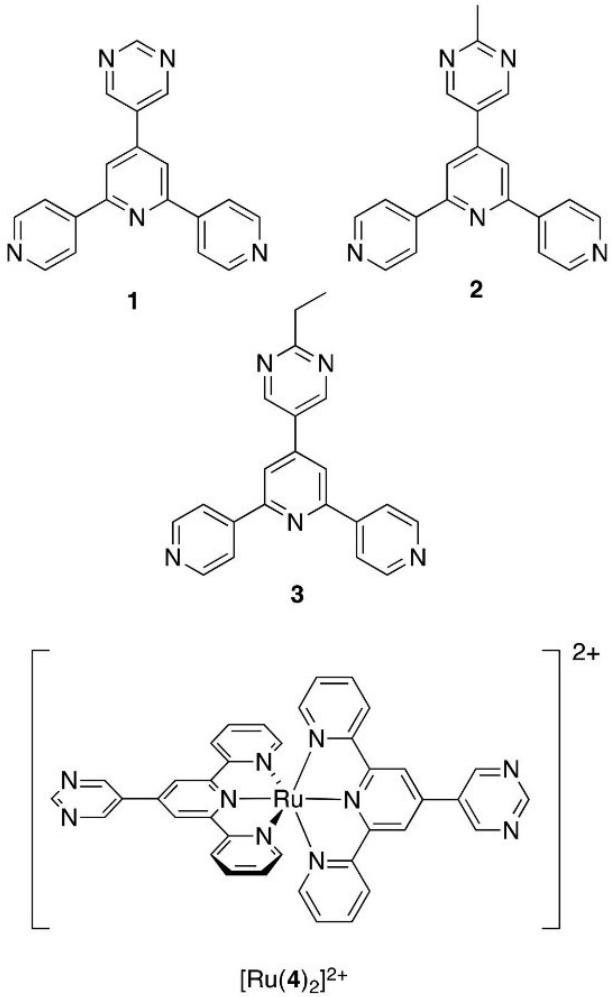

was synthesized in an analogous manner using the one-pot methodology of Hanan.[13] The electrospray mass spectrum of **3** showed a base peak at m/z 340.23 corresponding to $[M+H]^+$. The ^1H and ^{13}C NMR spectra of **3** (Figures S1 and S2) were assigned by COSY, NOESY, HMQC, and HMBC methods and were in accord with the structure shown in Chart 3.

Assembly in Solution of a 1D Coordination Polymer and a 2D Net. Reactions of ligands **1**, **2**, or **3** with copper(II) acetate or copper(I) triflate were investigated by room-temperature crystal growth experiments by layering a MeOH solution of each copper salt over a $CHCl_3$ solution of the ligand. X-ray-quality crystals $[Cu_2(OAc)_4(3)]_n$ and $\{[Cu(3)(OMe)(MeOH)][CF_3SO_3]\cdot MeOH\}_n$ were obtained after 1−2 weeks. Their structures illustrate the roles that the counterion (actetate or triflate) and solvent play in directing the coordination assembly.

$[Cu_2(OAc)_4(3)]_n$ comprises paddle-wheel $\{Cu_2(\mu\text{-}OAc)_4\}$ units linked by molecules of **3** which coordinate through the outer N atoms of the 4,2′:6′,4″-tpy unit (Figure S3). The coordination polymer crystallizes in the monoclinic $C2/c$ space group, and the asymmetric unit contains one $Cu(OAc)_2$ unit and half of one ligand **3**. The second half of the paddle-wheel motif is generated by inversion, and the second half of the 4,2′:6′,4″-tpy unit by 2-fold rotation. The 2-ethylpyrimidinyl unit is disordered with one complete half-occupancy ring and ethyl group in the asymmetric unit (as depicted in Figure S3) and the second half-occupancy ring generated by rotation about a 2-fold axis. Selected bond parameters describing coordination at atom Cu1 are shown in the caption to Figure S3. The structure propagates in a zigzag chain (Figure 1a) and is related

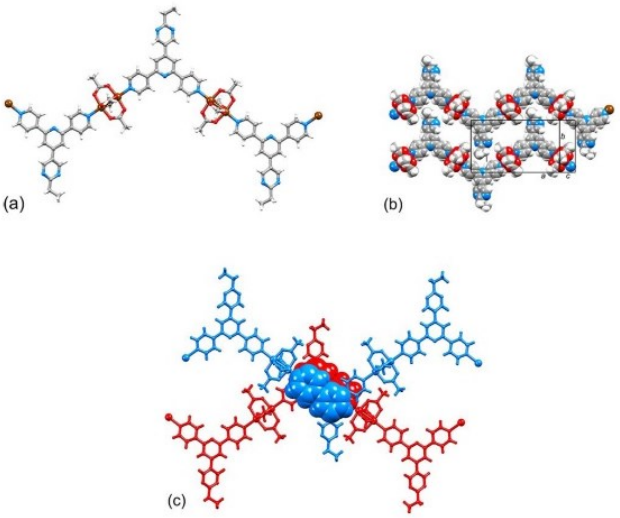

Figure 1. (a) Part of one zigzag chain in $[Cu_2(OAc)_4(3)]_n$. (b) Packing of adjacent chains to form a 2D sheet. (c) π-Stacking interactions between 4,2′:6′,4″-tpy domains in chains in adjacent sheets.

to a series of coordination polymers containing 4′-substituted 4,2′:6′,4″-tpy's and supported by $\{Cu_2(\mu\text{-}OAc)_4\}$ or $\{Zn_2(\mu\text{-}OAc)_4\}$ paddle-wheel nodes.[23,29−34] The zigzag chains pack into 2D sheets with the 2-ethylpyrimidinyl unit nestling into the V-shaped cavity offered by the 4,2′:6′,4″-tpy unit of an adjacent chain (Figure 1b). Finally, 2D sheets are associated through π-stacking interactions between 4,2′:6′,4″-tpy units in different chains (Figure 1c). Pairs of pyridine rings containing $N1^i/N2$ in one 4,2′:6′,4″-tpy and $N1^{iii}/N2^{iv}$ in an adjacent 4,2′:6′,4″-tpy (symmetry codes: i = $1-x$, y, $^3/_2-z$; iii = x, $1-y$, $^1/_2+z$; iv = $1-x$, $1-y$, $2-z$) are related by inversion and adopt an offset orientation (Figure 1c) typical of an efficient face-to-face π-stack.[35] The distance between the planes of pairs of stacked pyridine rings is 3.32 Å, and the inter-centroid separation is 3.64 Å. The assembly of chains in $[Cu_2(OAc)_4(3)]_n$ is predicated upon paddle-wheel $\{Cu_2(\mu\text{-}OAc)_4\}$ units acting as 2-connecting nodes,[9,36,37] and in $[Cu_2(OAc)_4(3)]_n$ the acetate anions play a crucial role as bridging ligands in the $\{Cu_2(\mu\text{-}OAc)_4\}$ nodes contributing fundamentally to the assembly process.

Layering a MeOH solution of copper(I) triflate over a $CHCl_3$ solution of **3** resulted in X-ray quality blue needles. The color suggested aerial oxidation to copper(II) as confirmed by the single crystal structure of $\{[Cu(3)(OMe)(MeOH)][CF_3SO_3]\cdot MeOH\}_n$. The compound crystallizes in the monoclinic space group $P2_1/n$, and Figure S4 depicts the repeat unit in the extended structure. Ligand **3** coordinates to Cu1 and the symmetry-generated $Cu1^i$ (see Figure S4 caption) through the outer two nitrogens N1 and N3. Atoms N2, N4, and N5 in the central pyridine and pyrimidine rings, respectively, are non-coordinated. Atom Cu1 is in a square-based pyramidal environment (τ = 0.20)[38] bound in two,

DOI: 10.1021/jacs.7b12624
J. Am. Chem. Soc. 2018, 140, 2933−2939

mutually *cis*, basal sites to N3 and N3^{iii} of two different ligands **3**. The remaining basal sites are occupied by methoxy ligands which support a $\{Cu_2(\mu\text{-}OMe)_2\}$ unit. A MeOH molecule bound through O2 (Figure S4) occupies the axial site of Cu1. The $\{Cu_2(\mu\text{-}OMe)_2\}$ units act as planar, 4-connecting nodes linked by the 4,2′:6′,4′′-tpy domains of **3** to generate a 2D (4,4) net. A TOPOS[39] representation is shown in Figure 2a

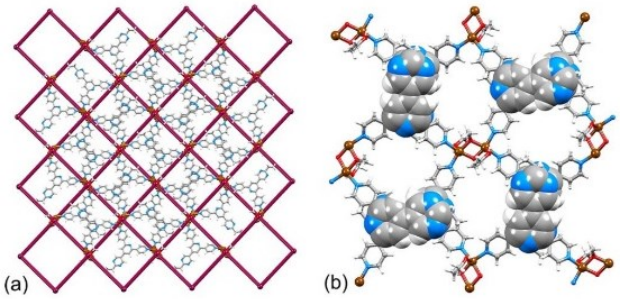

Figure 2. 2D network in $\{[Cu(\mathbf{3})(OMe)(MeOH)][CF_3SO_3]\cdot MeOH\}_n$: (a) TOPOS[39] representation with overlaid structure of part of one (4,4) net, and (b) part of one 2D sheet showing the π-stacking interactions between pyrimidin-5-ylpyridine units in adjacent ligands **3**.

with the molecular network overlaid. Within the 4,2′:6′,4′′-tpy unit, adjacent pyridine rings are twisted 14.9 and 30.7° with respect to one another. The plane of the pyrimidine ring is twisted only 7.0° with respect to the pyridine ring containing N2 (Figure S4). This near planarity is associated with face-to-face π-stacking of pyrimidin-5-ylpyridine units in adjacent ligands (Figure 2b). The stacked units are related by inversion and adopt an optimal offset arrangement.[35] The separation of the least-squares planes through the pyrimidin-5-ylpyridine units containing N2/N4/N5 and N2^{iv}/N4^{iv}/N5^{iv} is 3.48 Å, and the pyridine···pyrimidine centroid-to-centroid distance is 3.60 Å. The interactions lock the ligands into a compact 2D sheet, the cavities in which (Figure 2b) are occupied by triflate anions which exhibit short F···H and O···H contacts within the sheet. There are no π-stacking contacts between 2D sheets. In the assembly of $\{[Cu(\mathbf{3})(OMe)(MeOH)][CF_3SO_3]\cdot MeOH\}_n$, the choice of methanol as solvent plays a critical role, facilitating the formation of $\{Cu_2(\mu\text{-}OMe)_2\}$ units which are the 4-connecting nodes that direct the assembly of the 2D sheet.

■ ON-SURFACE ASSEMBLIES

The solution-based assemblies described above highlight not only the critical roles of solvent and counterions but also emphasizes the expected[27] coordination of **3** through only the outer N atoms of the 4,2′:6′,4′′-tpy domain. Solution-based coordination assemblies using 4′-(1*H*-imidazol-4-yl)-4,2′:6′,4′′-tpy (Chart 2) as the organic linker involve only the outer *N*-donors of the 4,2′:6′,4′′-tpy unit[26] but in contrast, the *N*-donors of the 4,2′:6′,4′′-tpy and imidazolyl units are involved in binding copper adatoms when the latter are added to an assembly of the ligand on an Au(111) surface.[25] We now demonstrate that this switch in coordination behavior is also observed for ligands **1**−**3**. Compounds **1**−**3**, differing only by the presence of an H, Me, or Et 2-substituent on the pyrimidin-5-yl functionality (Chart 3 and Figure 3) were deposited under UHV conditions by thermal sublimation. X-ray photoelectron spectroscopy (XPS) data were used to confirm that the compounds were deposited without chemical change by

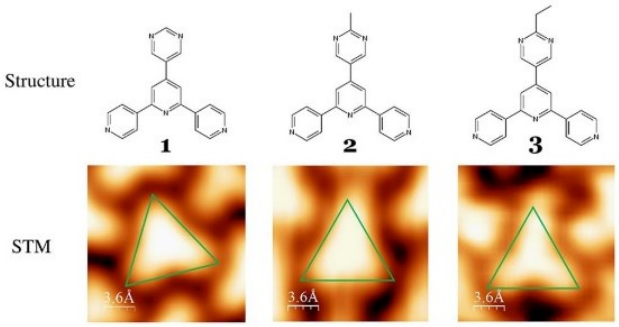

Figure 3. Structures and corresponding STM micrographs of compounds **1**, **2**, and **3** on a Au(111) substrate taken at 5 K with clearly distinguishable alkyl vertices allowing assignment of orientation. An equilateral triangle has been superimposed onto each image to guide the eye toward the different STM contrasts for the molecules. An enlarged version of the figure is given in Figure S7.

analyzing the relative ratios of the (deconvoluted) peaks (see Figure S6). Molecule **1** defines an equilateral triangle, whereas in **2** and **3**, the alkyl substituents act as an "imaging group" in the scanning tunneling microscopy (STM) images shown in Figures 3 and S7. Thus, as the substituent increases in size, it is possible to visualize molecular orientation.

When deposited on the inert surface of Au(111), **1** and **2** arrange in extended close-packed phases (Figures 4 and S8, top) attributed to the symmetry of the molecules, allowing for high packing densities in 2D arrangements. Differently oriented domains are separated by two types of boundaries, depending on the relative orientations of two domains (zipper-like or avoiding). In addition to weak non-classical C−H···N hydrogen-bond interactions,[40] attractive dipole forces are balanced by repulsive H···H interactions. The larger, and less symmetrical, ethyl substituent in **3** increases the "footprint" of the molecule and causes a looser 2D assembly while maintaining the principal assembly motifs. The ethyl groups are located in the so-formed cavity (Figure 4, top right) giving rise to highly

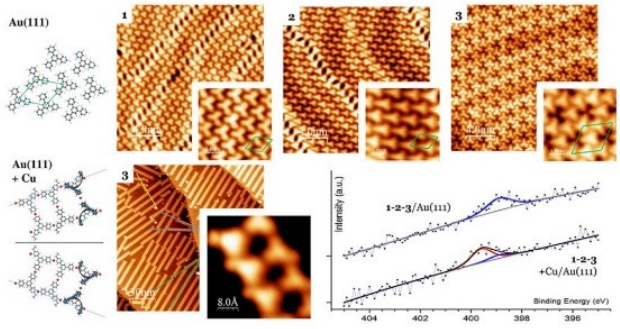

Figure 4. Molecules on Au(111) substrate. Top row: before Cu-coordination, **1** and **2** assemble into a close-packed layer, whereas **3** forms a regular porous vacancy pattern; each 5 × 5 nm inset shows the unit cell in green to emphasize the influence of the substituent on the 2D assembly. Bottom left: after Cu-coordination, 1D ladder-like structures assemble. The expansion shows that the ethyl groups point to the outside of the ladder. Chains are oriented in six directions, five of which are shown and indicated as blue, green, and yellow lines. Bottom right, XPS data showing the chemical change in the N environment, indicating metal coordination of the outer N (red line), while the inner pyridine-ring N of the tpy unit remains unchanged (blue line). An enlarged version of the figure is given in Figure S8.

DOI: 10.1021/jacs.7b12624
J. Am. Chem. Soc. 2018, 140, 2933−2939

structured alternating lines in three principal directions. This space-optimizing is reflected in the unit-cells of the assemblies, marked in green in the insets in Figure 4. The unit cell of **1** is 1 × 1 nm = 1 nm^2, of **2** is 1 × 1.25 nm = 1.25 nm^2, and of **3** is 2.05 × 2.05 nm = 4.20 nm^2 consistent with going from a pyrimidinyl to 2-methylpyrimidinyl to 2-ethylpyrimidinyl substituent. The unit cells of the adlayer exhibit a 60°/120°symmetry (see model Figure 4, as well as the insets) which is broken by the superposition with the Au(111)22×$\sqrt{3}$ reconstruction (*vide infra*).

The *in situ* addition of Cu-adatoms from a thermal evaporation source to the molecular assemblies of **1**, **2**, or **3** on Au(111) at room temperature results, in each case, in the formation of long, straight ladder-like chains. For **3** this is shown in Figure 4, and a comparison of the assemblies for all three ligands is shown in Figure S9, top. To investigate the origin of the re-organization of the on-surface assembly, XPS data were acquired before and after the addition of copper atoms. The peak at 398.9 eV marked in blue in Figures 4 and S8 arises from the uncoordinated N atoms. As we have previously shown,[25] the N atom of the central ring of the 4,2′:6′,4″-tpy unit does not coordinate, confirmed by the retention of the peak at 398.9 eV after Cu adatoms have been supplied. The XPS spectra are consistent with coordination to copper of both the outer *N*-donors of the 4,2′:6′,4″-tpy unit and the two pyrimidinyl N atoms, with the ratio of the new peak at 399.6 eV (shown in red in Figure 4 or Figure S10) to the peak at 398.9 eV being 4:1.

The assembly of the ladder-like arrays arises from the rearrangement of the molecules to optimize coordination to the Cu adatoms, and leads to 1D coordination double-chains (see model Figure 5 for more detail). The assemblies appear to be

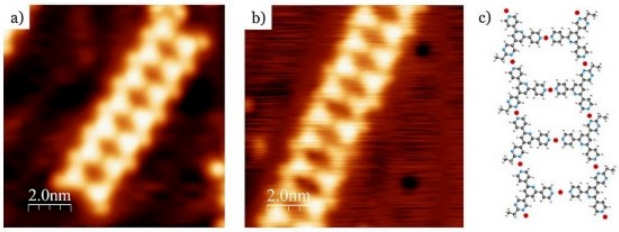

Figure 5. Comparison of ladders of **3** on (a) Au(111)+Cu adatoms and (b) Cu(111). The assemblies are also similar for **1** and **2** (see Figure S7 for full matrix). (c) Model of part of one chain showing the ethyl substituent pointing to the outside of the ladder. An enlarged version of the figure is given in Figure S12.

robust since the ladders remain straight and periodic across the complex domain pattern of the Au(111)22×3 reconstruction. This well-known surface reconstruction occurs due to a reorganization of the top layer of the gold substrate under strain, resulting in herringbone shaped striped domains with different stacking, hcp vs fcc of the top layer Au atoms on the fcc crystal below. The domain walls of the reconstructed Au top layer atoms in between these domains are slightly elevated and visualized in STM as a herringbone pattern.[41,42] The structural models in Figures 4 and S8 reflect what can be seen in the STM data after identification of the substituents of **2** and **3** which point to the outside of the ladders and are most clearly seen in the enlargement of the STM image of **3**. Each unit cell involves three Cu adatoms; in other words, three of the four coordinated N atoms share a Cu adatom with an N atom of a neighboring molecule (marked as red dots). Additionally, due to the orientation of the molecule within the ladder, both left- and right-handed chiralities are present in the three directions related by 120° (see yellow, blue, and green lines in the middle image of the bottom row in Figure 4; only five of the six directions are within the frame shown). The angle between ladders of opposite chiralities formed upon adsorption on the substrate depends on the molecular building block and is 20° for **3** and 38° for **2**. There is no evidence from either XPS or the STM analysis that Au adatoms from the substrate are involved in the formation of similar ladder-like assemblies.[43]

Deposition of ligands **1**−**3** was also carried out on a Cu(111) substrate held at room temperature (see Figure S11 for XPS multilayer result) which provides Cu adatoms for coordination from the surface during preparation.[44−46] Even though the change of substrate from Au(111) to Cu(111) involves a change in lattice constant, we observe a remarkable consistency in the morphology of both assemblies (Figures 5 and S12 versus Figure S9). The appearance of the same ladder-like assemblies testifies to this being a robust motif, and any differences between Cu(111) and Au(111) surfaces are within the error of the measurements. The chain width coincidentally is 2.3 nm (23 Å) on both substrates, which is equivalent to 8 × 2.88 Å (gold lattice constant) or 9 × 2.56 Å (copper lattice constant). The lack of dependence of the core assembly on the substituent is remarkable. As observed on Au(111), the ladders on Cu(111) also reveal their chirality, although in this case, all three functionalities (with **1**, **2**, or **3**) have the same 13 ± 1° chirality angle. All molecules in one strand are oriented in one direction, while all molecules from the other strand point in the opposite direction. No achiral ladders were observed.

As displayed in Figure S13, ladders can reach remarkable lengths of over 125 nm. The discontinuities visible in the chains (e.g., Figures 6 and S14, top left) are attributed to a jump in the

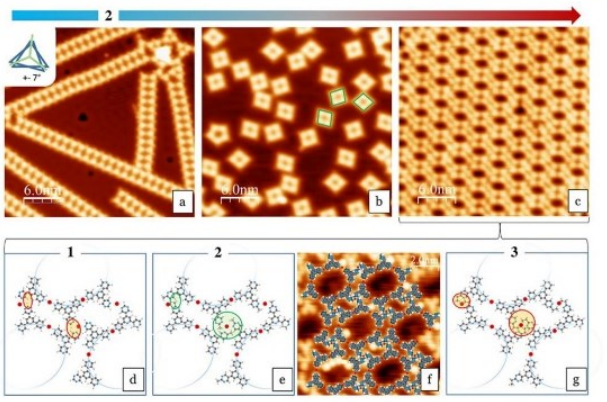

Figure 6. Sequential surface rearrangement. Top: Annealing sequence of **2** (RT, 20 min @ 240 °C, additional 20 min @ 290 °C). Ladders and tetramers are found for all three molecules **1**−**3**, but only **2** forms the porous network. Bottom: Closer examination of quasi-hexagon nanoporous network formation. (d) R = H: high repulsive H···H interactions. (e) R = Me: the ideal case, where in-plane hydrogen is positioned in-between tetrahedral oriented neighbors. (f) Space-filling models of **2** superimposed on a high-quality STM micrograph (base of the models) (recorded with Xe functionalized tip, with single Xe atoms visible as bright protrusions). (g) R = Et: repulsion between the Et groups leads to less efficient packing. For simplicity, non-relevant Cu adatoms have been omitted. An enlarged version of the figure is given in Figure S14.

DOI: 10.1021/jacs.7b12624
J. Am. Chem. Soc. 2018, 140, 2933−2939

registry in a lateral direction of one row on the Cu(111) substrate. The 2D assemblies of ladders are stable up to room temperature, but structural perturbation was achieved by annealing on the Cu(111) substrate. In a first stage, the ladders were transformed to tetramers (20 min at 240 °C, Figure 6b), and after further annealing for 20 min at 290 °C, hexagonal motifs were formed (Figure 6c). These hexagonal assemblies could also be obtained in a single annealing step of 30 min at 240 °C.

The tetramers exhibit three distinct orientations, related by 120° rotations (see the three tetramers highlighted in green in Figures 6b and S14b). For the rhombi, the internal angles are consistently 80/100°, due to the mismatch of square assemblies on a hexagonally oriented substrate. As with the ladder assemblies, the structure is not dependent on the substituents in **1**, **2**, and **3**, which are directed outside the assembly motif (rhombus side length of 2.3 nm ± 0.1 nm; see Figure S15 for a detailed comparison). A similar result is observed when directly depositing **1**, **2**, or **3** on a hot Cu(111) substrate, omitting the ladder assembly. Due to the availability of Cu adatoms at higher temperatures,[47] there is a smaller tendency for the organic molecules to share the Cu adatoms with their neighbors. This results in a preference for discrete tetramers over ladders. Per tetrameric motif, four Cu adatoms are involved in bonding forming a [4+4] metallomacrocyclic unit. This results in two shared adatoms per molecule in comparison to three for the ladders (see Figure S15 for a detailed model).

Unexpectedly, further annealing of the tetramers on Cu(111) with ligand **2** results in a further rearrangement into the nanoporous network seen in Figures 6c and S14c. Within the series of molecules **1**−**3**, the most compact packing is obtained with the methyl substituent (Figures 6 and S14, bottom row); in the analogous assembly formed with **1**, repulsive interactions involving H2 would destabilize this arrangement, whereas with **3** the ethyl has too great a steric demand.[48,49] It is remarkable, how small changes in the alkyl substituent result in such dramatic effects on the surface assembly. The nanoporous assembly of **2** (Figure 6c) is present in both chiral forms (see Figure S16).

Temperature dependent XPS analysis was carried out, revealing neither an annealing dependency of the on-surface assembly (see first column of Figure S17; in line with the result of **1**, **2**, **3** on Au(111) + Cu adatoms where full coordination already takes place at room temperature) nor compound dependency (see right column of Figure S17 for **2** vs **3** comparison; for all compounds N 1s peaks are at ∼398.6 and 399.7 (±0.2) eV). This result shows that the different behavior of **1**, **2**, and **3** is not based on differing chemical reactivity, but rather on the steric demand of the substituents. Tables S1 and S2 give a detailed XPS summary.

■ CONCLUSIONS

In conclusion, we have adopted an unconventional approach to metal−organic architectures by investigating how a common pair of ligand and metal responds to assembly in solution under ambient conditions or on a Au(111) or Cu(111) surface under UHV conditions. In solution, ligand **3** combines with copper(II) acetate or copper(I) triflate in MeOH to yield single crystals of, respectively, $[Cu_2(OAc)_4(\mathbf{3})]_n$ or $\{[Cu(\mathbf{3})(OMe)(MeOH)][CF_3SO_3]\cdot MeOH\}_n$. In the former, the acetate anions are critical to the formation of paddle-wheel $\{Cu_2(\mu\text{-}OAc)_4\}$ units which act as linear nodes and direct the assembly of 1D zigzag chains. In the latter, the methanol solvent is involved in the assembly of $\{Cu_2(\mu\text{-}OMe)_2\}$ units which act as planar, 4-connecting nodes connected by ligands **3** to generate a 2D (4,4) net. The roles of solvent and counteranion are negated by moving from solution to surface assemblies under vacuum. The different R groups in **1**, **2**, or **3** have been used as an imaging tool for STM. The difference in the substitution is visible in the close-packed phase on Au(111). After deposition of Cu adatoms, regular (ladder-shaped) surface metal−organic motifs assemble on the Au(111) surface and in all cases exhibit the same backbone structure, indicating the assembly is not influenced by the substituent. The ladder structure also assembles on Cu(111) where Cu adatoms are available during the deposition and subsequent relaxation process at room temperature. With progressively increasing annealing temperature, the original surface assemblies are modified and undergo a transition from ladders into rhomboid structures, and for ligand **2**, a quasi-hexagonal nanoporous network is observed.

Although both the assembly in solution and the solvent-free coordination assembly in vacuum provide coordination assemblies featuring planar layers, there is an important difference. The Cu coordination center in the case of the solution assembly follows the rules of coordination chemistry while the substrate-supported Cu coordination centers also show other more planar motifs, stabilized by the coordinated metal atom interacting with the underlying substrate. It is also interesting to note that this "surface-supported" Cu coordination does not appear to depend on whether Au(111) or Cu(111) substrates are used. The inclusion of counterions and solvent molecules in the lattice determines that bulk crystalline material and surface assemblies differ in their microstructures, motivating further in depth investigations. It is remarkable, however, that the general principles and algorithms determining the structures of solution-grown crystalline material can be extended to surface assemblies.

■ ASSOCIATED CONTENT

Supporting Information

The Supporting Information is available free of charge on the ACS Publications website at DOI: 10.1021/jacs.7b12624.

Experimental details; NMR spectra; ORTEP-style figures; powder diffraction data; enlarged versions of manuscript figures and additional STM images; XPS analysis (PDF)

X-ray crystallographic data for $[Cu_2(OAc)_4(\mathbf{3})]_n$ (CIF)

X-ray crystallographic data for $\{[Cu(\mathbf{3})(OMe)(MeOH)][CF_3SO_3]\cdot MeOH\}$ CIF)

■ AUTHOR INFORMATION

Corresponding Authors

*catherine.housecroft@unibas.ch

*thomas.jung@psi.ch

ORCID

Sylwia Nowakowska: 0000-0001-9463-7640

Catherine E. Housecroft: 0000-0002-8074-0089

Thomas A. Jung: 0000-0003-0717-9886

Notes

The authors declare no competing financial interest.

■ ACKNOWLEDGMENTS

We thank the Swiss National Science Foundation (grant numbers 200020-162631, 200020-149713, and 206021-121461), the Swiss Nanoscience Institute P1203, the Swiss Commission for Technology and Innovation (CTI, 16465.1 PFNM-NM), and the Swiss Government Excellence Scholarship Program for Foreign Scholars, as well as the University of Basel for financial support. Dr. Markus Neuburger (University of Basel) is thanked for assistance with single-crystal structure determinations, Aneliia Wäckerlin (University of Basel) for initial assistance and discussions, Mariah O'Doherty (Trinity College, Dublin) for assisting with the STM experiments and for helpful discussions, and Marco Martina and Matthes Senn (University of Basel) for technical support.

■ REFERENCES

(1) Constable, E. C. *Adv. Inorg. Chem.* **2018**, DOI: 10.1016/bs.adioch.2017.11.005.
(2) Constable, E. C. *Chem. Ind.* **1994**, 56.
(3) Housecroft, C. E.; Sharpe, A. G. *Inorganic Chemistry*, 4th ed.; Pearson Education Ltd.: Harlow, UK, 2012.
(4) Batten, S. R.; Neville, S. M.; Turner, D. R. *Coordination Polymers: Design, Analysis and Application*; RSC Publishing, Cambridge, UK, 2009.
(5) See, for example: Kang, Z.; Fan, L.; Sun, S. *J. Mater. Chem. A* **2017**, *5*, 10073. Huang, Y.-B.; Liang, J.; Wang, X.-S.; Cao, R. *Chem. Soc. Rev.* **2017**, *46*, 126. Canivet, J.; Vandichel, M.; Farrusseng, D. *Dalton Trans.* **2016**, *45*, 4090. Liu, J.; Woll, C. *Chem. Soc. Rev.* **2017**, *46*, 5730. Li, B.; Wen, H.-M.; Cui, Y.; Zhou, W.; Qian, G.; Chen, B. *Adv. Mater.* **2016**, *28*, 8819. Furukawa, H.; Cordova, K. E.; O'Keeffe, M.; Yaghi, O. M. *Science* **2013**, *341*, 974. Schoedel, A.; Li, M.; Li, D.; O'Keeffe, M.; Yaghi, O. M. *Chem. Rev.* **2016**, *116*, 12466.
(6) Spillmann, H.; Kiebele, A.; Stöhr, M.; Jung, T. A.; Bonifazi, D.; Cheng, F.; Diederich, F. *Adv. Mater.* **2006**, *18*, 275.
(7) Nowakowska, S.; Wäckerlin, A.; Kawai, S.; Ivas, T.; Nowakowski, J.; Fatayer, S.; Wäckerlin, C.; Nijs, T.; Meyer, E.; Björk, J.; Stöhr, M.; Gade, L. H.; Jung, T. A. *Nat. Commun.* **2015**, *6*, 6071.
(8) Nowakowska, S.; Wäckerlin, A.; Piquero-Zulaica, I.; Nowakowski, J.; Kawai, S.; Wäckerlin, C.; Matena, M.; Nijs, T.; Fatayer, S.; Popova, O.; Ahsan, A.; Mousavi, S. F.; Ivas, T.; Meyer, E.; Stöhr, M.; Ortega, J. E.; Björk, J.; Gade, L. H.; Lobo-Checa, J.; Jung, T. A. *Small* **2016**, *12*, 3757.
(9) Constable, E. C. *Chem. Soc. Rev.* **2007**, *36*, 246.
(10) Housecroft, C. E. *Dalton Trans.* **2014**, *43*, 6594.
(11) Housecroft, C. E. *CrystEngComm* **2015**, *17*, 7461.
(12) Kröhnke, F. *Synthesis* **1976**, *1976*, 1.
(13) Wang, J.; Hanan, G. S. *Synlett* **2005**, *2005*, 1251.
(14) Klein, Y. M.; Prescimone, A.; Pitak, M. B.; Coles, S. J.; Constable, E. C.; Housecroft, C. E. *CrystEngComm* **2016**, *18*, 4704.
(15) Yin, Z.; Zhang, S.; Zheng, S.; Golen, J. A.; Rheingold, A. L.; Zhang, G. *Polyhedron* **2015**, *101*, 139.
(16) Li, X.-Z.; Zhou, X.-P.; Li, D.; Yin, Y.-G. *CrystEngComm* **2011**, *13*, 6759.
(17) Xi, Y.; Wei, W.; Xu, Y.; Huang, X.; Zhang, F.; Hu, C. *Cryst. Growth Des.* **2015**, *15*, 2695.
(18) Yuan, F.; Xie, J.; Hu, H.-M.; Yuan, C.-M.; Xu, B.; Yang, M.-L.; Dong, F.-X.; Xue, G.-L. *CrystEngComm* **2013**, *15*, 1460.
(19) Gong, Y.; Zhang, M. M.; Zhang, P.; Shi, H. F.; Jiang, P. G.; Lin, J. H. *CrystEngComm* **2014**, *16*, 9882.
(20) Yuan, F.; Zhu, Q.; Hu, H.-M.; Xie, J.; Xu, B.; Yuan, C.-M.; Yang, M.-L.; Dong, F.-X.; Xue, G.-L. *Inorg. Chim. Acta* **2013**, *397*, 117.
(21) Yang, J.; Yan, S.-W.; Wang, X.; Xiao, D.-R.; Zhang, H.-Y.; Chi, X.-L.; Zhang, J.-L.; Wang, E. *Inorg. Chem. Commun.* **2013**, *38*, 100.
(22) Chen, Y.-Q.; Li, G.-R.; Chang, Z.; Qu, Y.-K.; Zhang, Y.-H.; Bu, X.-H. *Chem. Sci.* **2013**, *4*, 3678.
(23) Constable, E. C.; Housecroft, C. E.; Neuburger, M.; Schönle, J.; Vujovic, S.; Zampese, J. A. *Polyhedron* **2013**, *60*, 120.
(24) Li, L.; Zhang, Y. Z.; Yang, C.; Liu, E.; Golen, J. A.; Zhang, G. *Polyhedron* **2016**, *105*, 115.
(25) Nijs, T.; Malzner, F. J.; Fatayer, S.; Wäckerlin, A.; Nowakowska, S.; Constable, E. C.; Housecroft, C. E.; Jung, T. A. *Chem. Commun.* **2015**, *51*, 12297.
(26) Constable, E. C.; Housecroft, C. E.; Neuburger, M.; Vujovic, S.; Zampese, J. A.; Zhang, G. *CrystEngComm* **2012**, *14*, 3554.
(27) Klein, Y. M.; Constable, E. C.; Housecroft, C. E.; Zampese, J. A. *Polyhedron* **2014**, *81*, 98.
(28) Beves, J. E.; Constable, E. C.; Decurtins, S.; Dunphy, E. L.; Housecroft, C. E.; Keene, T. D.; Neuburger, M.; Schaffner, S. *CrystEngComm* **2008**, *10*, 986.
(29) Constable, E. C.; Zhang, G.; Coronado, E.; Housecroft, C. E.; Neuburger, M. *CrystEngComm* **2010**, *12*, 2139.
(30) Constable, E. C.; Zhang, G.; Housecroft, C. E.; Neuburger, M.; Zampese, J. A. *CrystEngComm* **2010**, *12*, 2146.
(31) Constable, E. C.; Housecroft, C. E.; Kopecky, P.; Neuburger, M.; Zampese, J. A.; Zhang, G. *CrystEngComm* **2012**, *14*, 446.
(32) Constable, E. C.; Housecroft, C. E.; Vujovic, S.; Zampese, J. A.; Crochet, A.; Batten, S. R. *CrystEngComm* **2013**, *15*, 10068.
(33) Klein, Y. M.; Constable, E. C.; Housecroft, C. E.; Zampese, J. A.; Crochet, A. *CrystEngComm* **2014**, *16*, 9915.
(34) Zhang, G.; Jia, Y.-X.; Chen, W.; Lo, W.-F.; Brathwaite, N.; Golen, J. A.; Rheingold, A. L. *RSC Adv.* **2015**, *5*, 15870.
(35) Janiak, C. *J. Chem. Soc., Dalton Trans.* **2000**, 3885.
(36) Pariyar, A.; Stansbery, J.; Patel, R. L.; Liang, X.; Choudhury, A. *J. Coord. Chem.* **2016**, *69*, 1957.
(37) Köberl, M.; Cokoja, M.; Herrmann, W. A.; Kühn, F. E. *Dalton Trans.* **2011**, *40*, 6834.
(38) Addison, A. W.; Rao, T. N.; Reedijk, J.; van Rijn, J.; Verschoor, G. C. *J. Chem. Soc., Dalton Trans.* **1984**, 1349.
(39) Blatov, V. A.; Shevchenko, A. P. *ToposPro*, v. 4.0; Samara State University, Russia, 2005.
(40) Desiraju, G. R.; Steiner, T. *The Weak Hydrogen Bond in Structural Chemistry and Biology*; Oxford University Press, Oxford, UK, 1999.
(41) Wöll, Ch.; Chiang, S.; Wilson, R. J.; Lippel, P. H. *Phys. Rev. B: Condens. Matter Mater. Phys.* **1989**, *39*, 7988.
(42) Barth, J. V.; Brune, H.; Ertl, G.; Behm, R. J. *Phys. Rev. B: Condens. Matter Mater. Phys.* **1990**, *42*, 9307.
(43) Pham, T. A.; Song, F.; Alberti, M. N.; Nguyen, M.-T.; Trapp, N.; Thilgen, C.; Diederich, F.; Stöhr, M. *Chem. Commun.* **2015**, *51*, 14473.
(44) Lin, N.; Payer, D.; Dmitriev, A.; Strunskus, T.; Wöll, C.; Barth, J. V.; Kern, K. *Angew. Chem., Int. Ed.* **2005**, *44*, 1488.
(45) Pawin, G.; Wong, K. L.; Kim, D.; Sun, D.; Bartels, L.; Hong, S.; Rahman, T. S.; Carp, R.; Marsella, M. *Angew. Chem., Int. Ed.* **2008**, *47*, 8442.
(46) Sirtl, T.; Schlögl, S.; Rastgoo-Lahrood, A.; Jelic, J.; Neogi, S.; Schmittel, M.; Heckl, W. M.; Reuter, K.; Lackinger, M. *J. Am. Chem. Soc.* **2013**, *135*, 691.
(47) Lin, N.; Payer, D.; Dmitriev, A.; Strunskus, T.; Wöll, C.; Barth, J. V.; Kern, K. *Angew. Chem., Int. Ed.* **2005**, *44*, 1488.
(48) Wintjes, N.; Hornung, J.; Lobo-Checa, J.; Voigt, T.; Samuely, T.; Thilgen, C.; Stöhr, M.; Diederich, F.; Jung, T. A. *Chem. - Eur. J.* **2008**, *14*, 5794.
(49) Enache, M.; Maggini, L.; Llanes-Pallas, A.; Jung, T. A.; Bonifazi, D.; Stöhr, M. *J. Phys. Chem. C* **2014**, *118*, 15286.

■ NOTE ADDED IN PROOF

We have become aware that the experimental results presented in this paper further confirm the structural models presented in P. Szabelski, W. Rżysko, and D. Nieckarz, *J. Phys. Chem. C* **2016**, *120*, 13139. We thank Professor Szabelski for making us aware of this publication.

DOI: 10.1021/jacs.7b12624
J. Am. Chem. Soc. 2018, 140, 2933−2939

Supplementary information to accompany:

The different faces of 4'-pyrimidinyl functionalized 4,2':6',4''-terpyridines: metal organic assemblies from solution and on Au(111) and Cu(111) surface platforms

Thomas Nijs,[a] Y. Maximilian Klein,[b] S. Fatemeh Mousavi,[a] Aisha Ahsan,[a] Sylwia Nowakowska,[a] Edwin C. Constable,[b] Catherine E. Housecroft[b]* and Thomas Jung[a,c]*

[a] Department of Physics, University of Basel, Klingelbergstrasse 82, 4056 Basel, Switzerland

[b] Department of Chemistry, University of Basel, BPR 1096, Mattenstrasse 24a 4058 Basel, Switzerland

[c] Laboratory for Micro- and Nanotechnology, Paul Scherrer Institut, 5232 Villigen, Switzerland.

Supplementary information

Experimental section

General. ^{1}H and ^{13}C NMR spectra were recorded on a Bruker DRX-500 NMR spectrometer with chemical shifts referenced to residual solvent peaks (TMS = δ 0 ppm). Electrospray ionisation (ESI) mass spectra were measured on a Bruker esquire 3000plus spectrometer or Shimadzu LCMS-2020 instrument, and high resolution ESI mass spectra on a Bruker maXis 4G QTOF instrument.

Compounds **1** and **2** were prepared as previously reported. [1] $Cu(OAc)_2{\cdot}H_2O$ and $Cu_2(CF_3SO_3)_2{\cdot}C_7H_8$ were purchased from Sigma Aldrich.

Compound 3

Structure of **3** with atom labelling for NMR spectroscopic assignments.

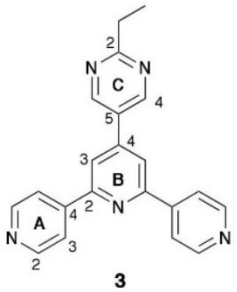

3

2-Ethylpyrimidine-5-carbaldehyde (0.5 g, 3.67 mmol) was dissolved in EtOH (80 mL), and 4-acetylpyridine (0.92 mL, 0.1 g, 8.07 mmol) was added followed by crushed solid KOH (0.52 g, 9.18 mmol). Aqueous NH_3 (25%, 18.1 mL, 117 mmol) was added dropwise and the mixture was stirred for ~15 h at ambient temperature. A white precipitate formed which was separated by filtration, washed with water (3 × 10 mL), EtOH (3 × 10 mL) and Et_2O (3 × 10 mL). Compound **3** was obtained as a white solid (0.21 g, 3.67 mmol, 16.8 %). M.p. = 275.3 °C. ^{1}H NMR (500 MHz, $CDCl_3$) δ / ppm 9.03 (s, 2H, H^{C4}), 8.82 (m, 4H, H^{A2}), 8.07 (m, 4H, H^{A3}), 8.01 (s, 2H, H^{B3}), 3.13 (q, J = 7.6 Hz, 2H, H^{Et}), 1.45 (t, J = 7.6 Hz, 3H, H^{Et}). $^{13}C\{^1H\}$ NMR (126 MHz, $CDCl_3$) δ / ppm 173.6 (C^{C2}), 156.1 (C^{A4}), 155.3 (C^{C4}), 150.9 (C^{A2}), 145.5 (C^{B2}), 145.3 (C^{B4}), 128.8 (C^{C5}), 121.3 (C^{A3}), 118.5 (C^{B3}), 32.7 (C^{Et}), 12.8 (C^{Me}). ESI-MS m/z 340.23 $[M+H]^+$ (calc. 340.16). High resolution ESI-MS m/z 340.1561 $[M+H]^+$ (calc. 340.1557)

$[Cu_2(OAc)_4(3)]_n$

A solution of $Cu(OAc)_2 \cdot H_2O$ (4.11 mg, 0.021 mmol) in MeOH (8 mL) was layered over a solution of **3** (7.0 mg, 0.021 mmol) in $CHCl_3$ (5 mL). Blue crystals of $[Cu_2(OAc)_4(\mathbf{3})]_n$ (0.9 mg, 0.00128 mmol, 12.2 % based on $Cu(OAc)_2$) were

obtained after 1–2 weeks. Insufficient amount of material was obtained for bulk sample analysis.

{[Cu(3)(OMe)(MeOH)][CF_3SO_3]·MeOH}$_n$

A solution of $Cu_2(CF_3SO_3)_2 \cdot C_7H_8$ (10.7 mg, 0.021 mmol) in MeOH (8 mL) was layered over a solution of **3** (7.0 mg, 0.021 mmol) in $CHCl_3$ (5 mL). Blue crystals of {[Cu(**3**)(OMe)(MeOH)][CF_3SO_3]·MeOH}$_n$ (5.4 mg, 0.00834 mmol, 39.7% based on **3**) were obtained after 1–2 weeks. The bulk material was characterized by powder diffraction.

Crystallography. Single crystal data were collected on a STOE StadiVari diffractometer equipped with a Pilatus300K detector and with a Metaljet D2 source; data reduction, solution and refinement used the programs STOE X-AREA, STOE X-RED, SuperFlip and CRYSTALS respectively.[2,3,4] Structure analysis used the programs Mercury v. 3.6[5,6] and TOPOS.[7] Powder diffraction data were collected on a Stoe Stadi P powder diffractometer.

[$Cu_2(OAc)_4$(**3**)]$_n$. $C_{29}H_{29}Cu_2N_5O_8$, M = 702.67, blue plate, monoclinic, space group $C2/c$, a = 26.0869(15), b = 14.8694(9), c = 8.1356(5) Å, β = 108.012(3)°, U = 3001.11(18) Å^3, Z = 4, D_c = 1.555 Mg m^{-3}, μ(Ga-Kα) = 2.248 mm^{-1}, T = 123 K. Total 29718 reflections, 2832 unique, R_{int} = 0.037. Refinement of 2686 reflections (236 parameters) with $I > 2\sigma(I)$ converged at final $R1$ =0.0495 ($R1$ all data = 0.0520), $wR2$ = 0.1250 ($wR2$ all data = 0.1261), gof = 1.0222. CCDC 1585047.

{[Cu(**3**)(OMe)(MeOH)][CF_3SO_3]·MeOH}. $C_{25}H_{28}CuF_3N_5O_6S$, M = 647.13, blue needle, monoclinic, space group $P2_1/n$, a = 7.3589(2), b = 19.2305(3), c = 19.2279(4) Å, β = 93.221(2)°, U = 2716.74(6) Å^3, Z = 4, D_c = 1.582 Mg m^{-3}, μ(Ga-

Kα) = 5.221 mm^{-1}, T = 123 K. Total 50738 reflections, 5511 unique, R_{int} = 0.065. Refinement of 4419 reflections (376 parameters) with $I > 2\sigma(I)$ converged at final $R1$ =0.04705 ($R1$ all data = 0.0577), $wR2$ = 0.0976 ($wR2$ all data = 0.1090), gof = 1.0087. CCDC 1585048.

On-surface study

In-situ sample preparation, scanning tunneling microscopy (STM) investigations and X-ray photoelectron spectroscopy (XPS) measurements (performed at the Paul Scherrer Institute (PSI), Laboratory for Micro- and Nanotechnology) were carried out under ultrahigh vacuum (UHV) conditions (base pressure of 5 x 10^{-11} mBar). Au(111) and Cu(111) crystals (MaTecK GmbH) were prepared by subsequent sputtering annealing cycles (Ar+ ions at 1 keV, 630 K respectively). Molecules were deposited by means of thermal evaporation from a commercial evaporator (Kentax GmbH) with sublimation temperatures of around 480 K. Metal adatoms were added by e-beam evaporator (Oxford Applied research). Quartz crystal microbalance was used to control the coverage. Sample preparation as well as XPS were performed at room temperature, whereas STM images were recorded at 5 K. Typical scanning parameters were 1 V and 10 pA, in constant current mode (Omicron Nanotechnology GmbH). STM tips (90% Pt, 10% Ir) were mechanically cut and sputtered *in-situ* with Ar+ ions. For XPS, was a monochromatic Al kα X-ray source with a full width at half maximum (FWHM) of 1.2 eV was used. As analysis software was used WSxM[8] in case of STM and Unifit in case of XPS.

Supplementary Figures

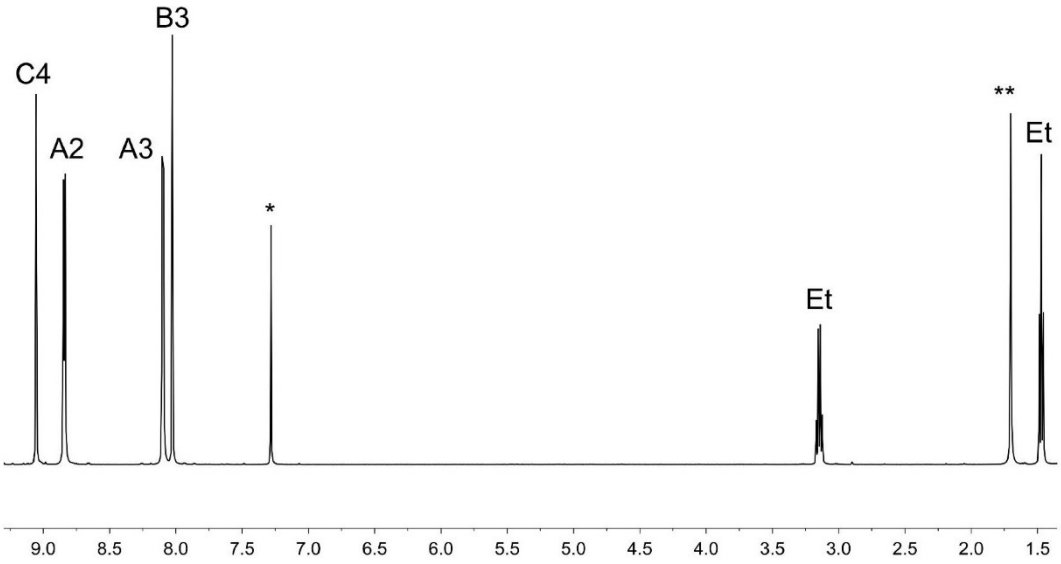

Fig. S1. 500 MHz ^{1}H NMR spectrum of **3** in $CDCl_3$. * = residual $CHCl_3$; ** = water.

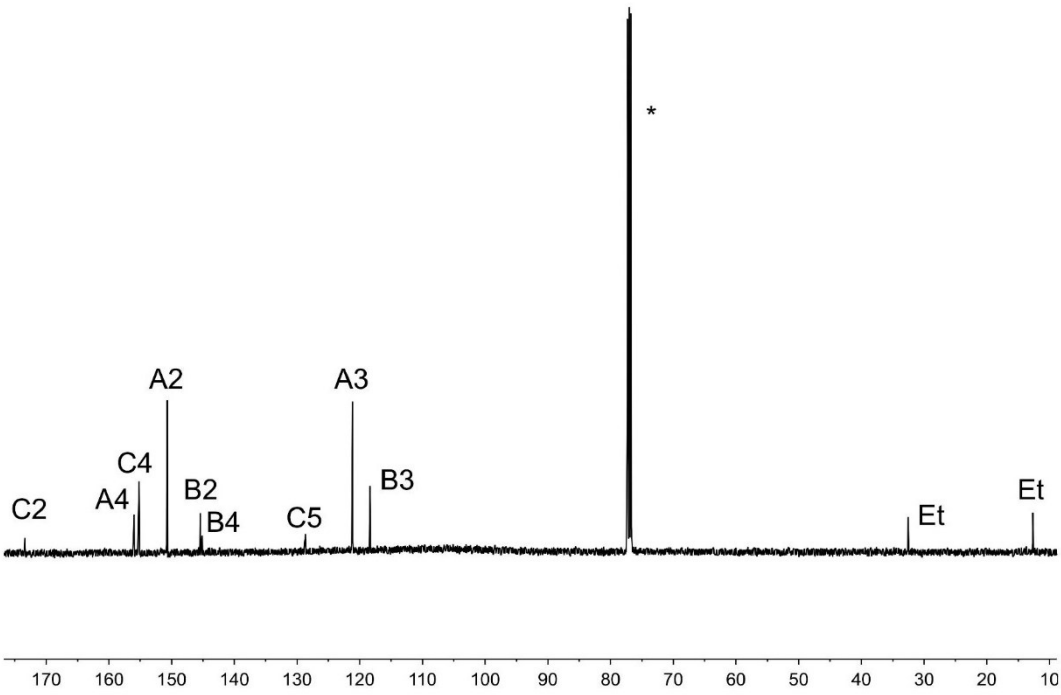

Fig. S2. 126 MHz ^{13}C NMR spectrum of **3** in $CDCl_3$. * = $CDCl_3$.

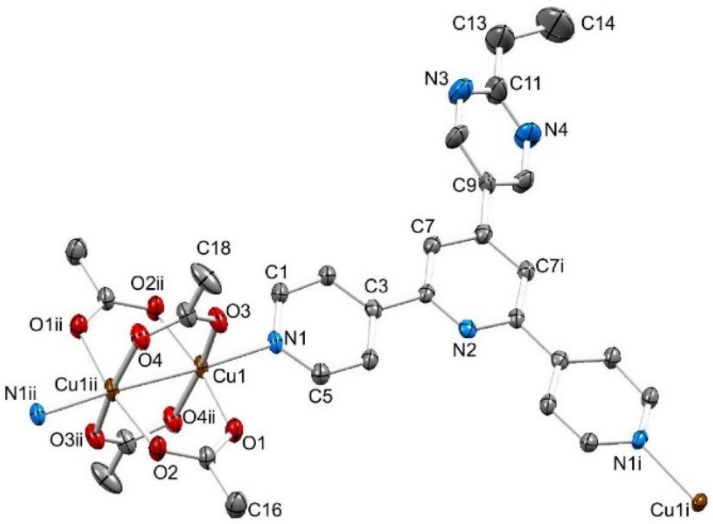

Fig. S3. Structure of the repeat unit (with symmetry generated Cu1i and N1ii atoms) in $[Cu_2(OAc)_4(\mathbf{3})]_n$ (ellipsoids plotted at 40% probability level and H atoms omitted); the ring containing N3 and N4 is disordered (see text). Symmetry codes: i = 1–*x*, *y*, $^3/_2$–*z*; ii = $^3/_2$–*x*, $^3/_2$–*y*, 1–*z*. Selected bond parameters: Cu1–N1 = 2.141(2), Cu1–O1 = 1.972(2), Cu1–O3 = 1.9750(19), Cu1–O4^{ii} = 1.9879(19), Cu1–O2^{ii} = 1.967(2), Cu1–Cu1^{ii} = 2.6096(7) Å; O4^{ii}–Cu1–N1 = 98.87(8), O2^{ii}–Cu1–N1 = 95.33(8), O1–Cu1–N1 = 95.67(8), O3–Cu1–N1 = 92.31(8)°.

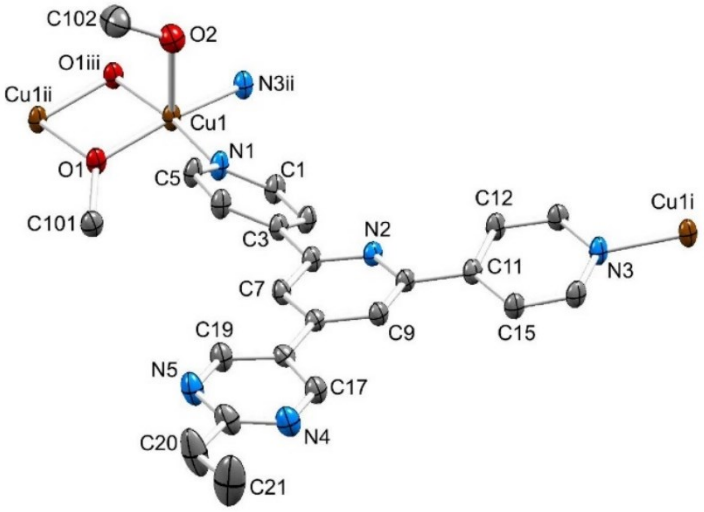

Fig. S4. Structure of the repeat unit (with symmetry generated atoms) in $\{[Cu(\mathbf{3})(OMe)(MeOH)][CF_3SO_3]\cdot MeOH\}_n$ (ellipsoids plotted at 40% probability level and H atoms omitted). Symmetry codes: i = $^3/_2$–*x*, $^1/_2$+*y*, $^1/_2$–*z*; ii = $^3/_2$–*x*, –$^1/_2$+*y*, $^1/_2$–*z*; iii = 2–*x*, 1–*y*, –*z*. Selected bond parameters: Cu1–N3^{ii} = 2.008(3), Cu1–O1 = 1.944(2), Cu1–O1^{iii} = 1.946(2), Cu1– N1 = 2.008(2), Cu1–O2 = 2.301(3), Cu1–Cu1^{ii} = 3.0454(8) Å; N1–Cu1–O1 = 93.69(10), N1–Cu1–O2 = 87.27(11), O1–Cu1–O2 = 105.10(10), N3^{ii}–Cu1–O1^{iii} = 92.67(9), N3^{ii}–Cu1–N1 = 97.14(10), O1^{iii}–Cu1–O1 = 76.95(9), N3^{ii}–Cu1–O2 = 94.15(11), O1^{iii}–Cu1–O2 = 92.25(10), N3^{ii}–Cu1–O1 = 158.33(11), O1^{iii}–Cu1–N1 = 170.18(10)°.

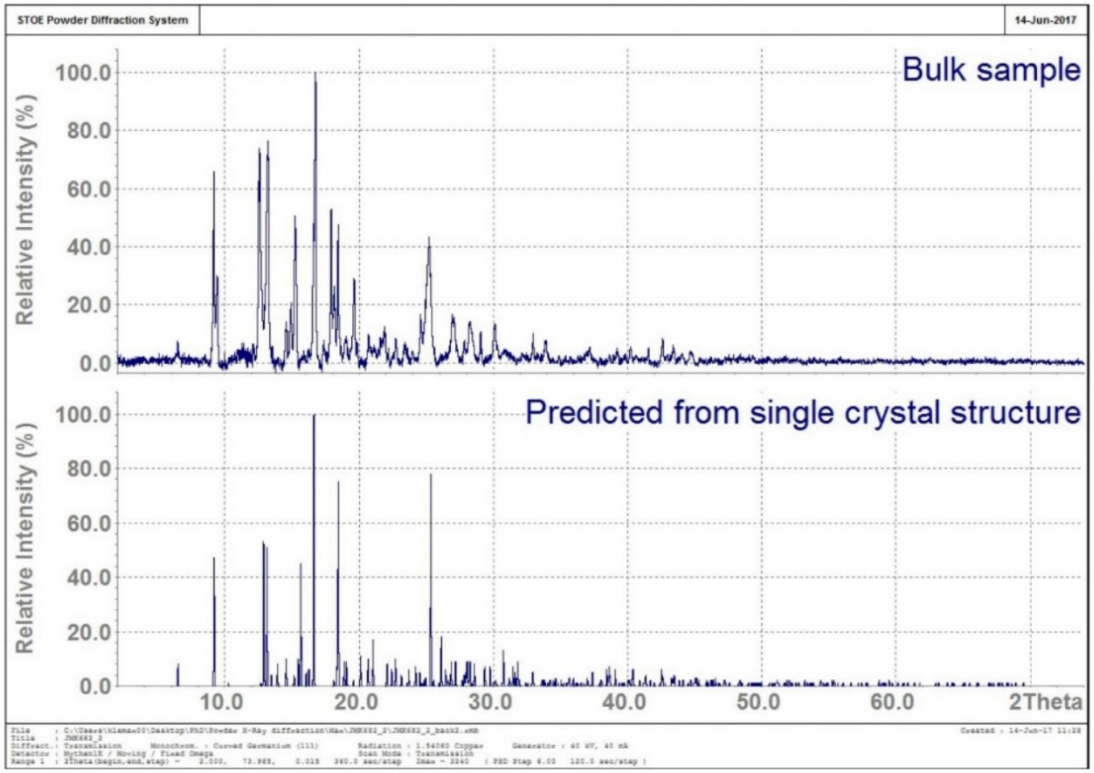

Fig. S5. Comparison of the powder diffraction patterns of the bulk sample obtained from the reaction of $Cu_2(CF_3SO_3)_2$ and **3** (top) and that predicted from the single crystal structure of $\{[Cu(\mathbf{3})(OMe)(MeOH)][CF_3SO_3]\cdot MeOH\}_n$ (123 K).

S7

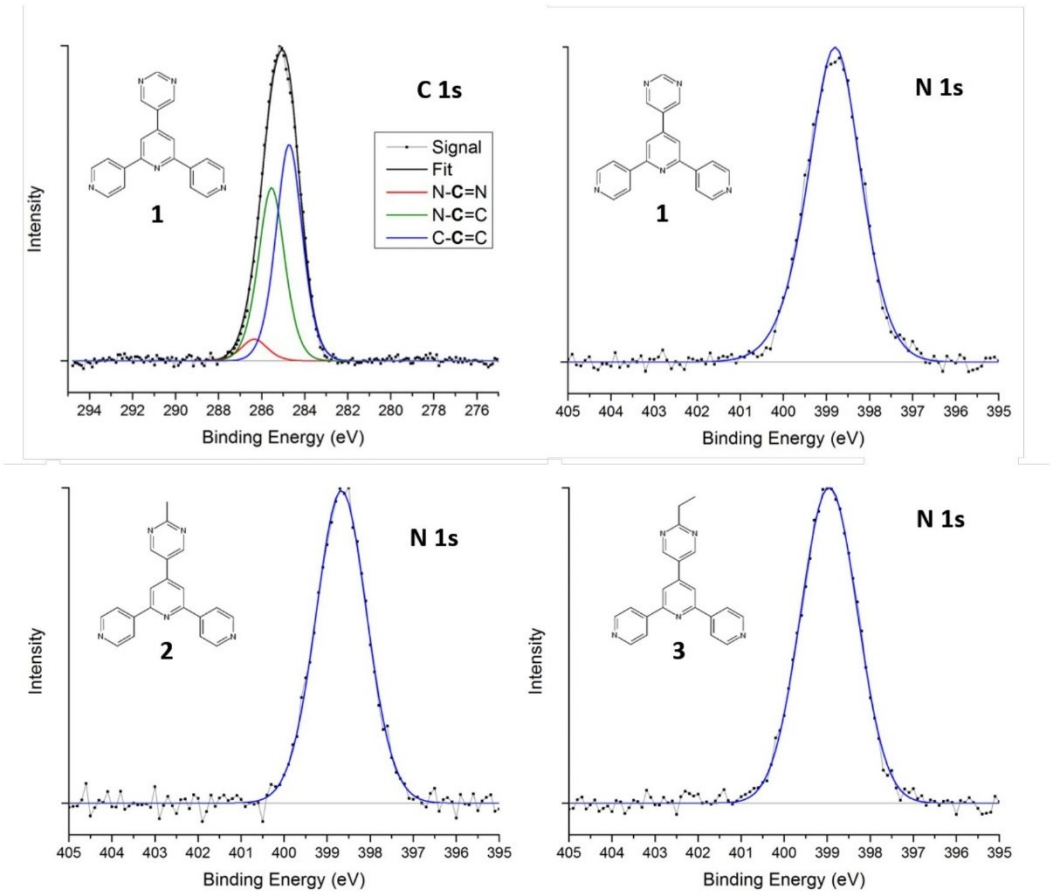

Fig. S6. XPS analysis of multilayer of **1, 2, 3** on Au(111) indicates sublimation of intact compounds. The C 1s vs. N 1s peak ratio as well as the detailed deconvolution of the C 1s peak provide the correct stoichiometry. The N 1s peak is situated at 398.8 ± 0.1 eV for all 3 compounds, consistent with coordination.

(**1**): C:C:C = 1:8:10. Total N:C ratio => 1:3.7. (Example shown)

(**2**): C:C:C = 1:8:11. Total N:C ratio => 1:4.0.

(**3**): C:C:C = 1:8:12. Total N:C ratio => 1:4.2.

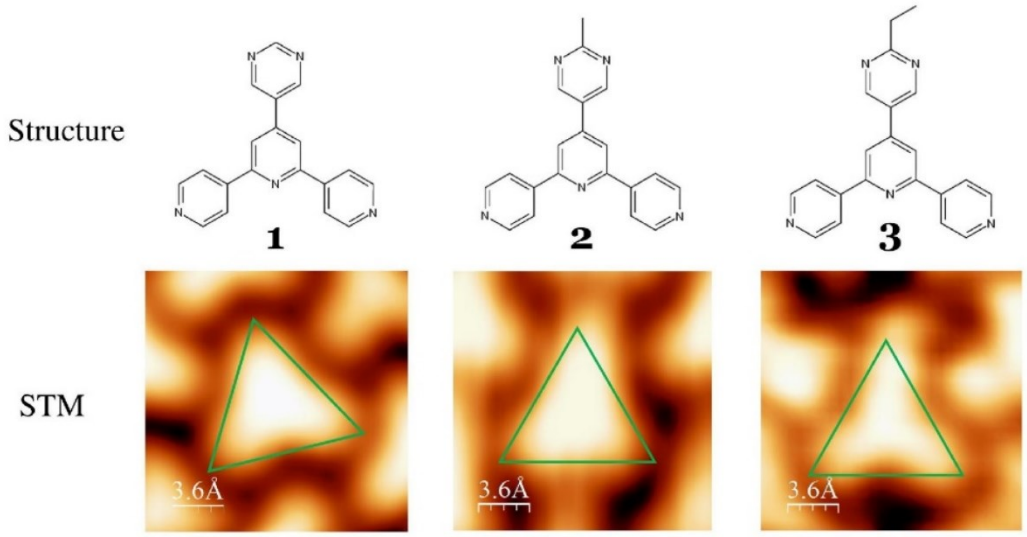

Fig. S7. Enlargement of manuscript Fig. 3.

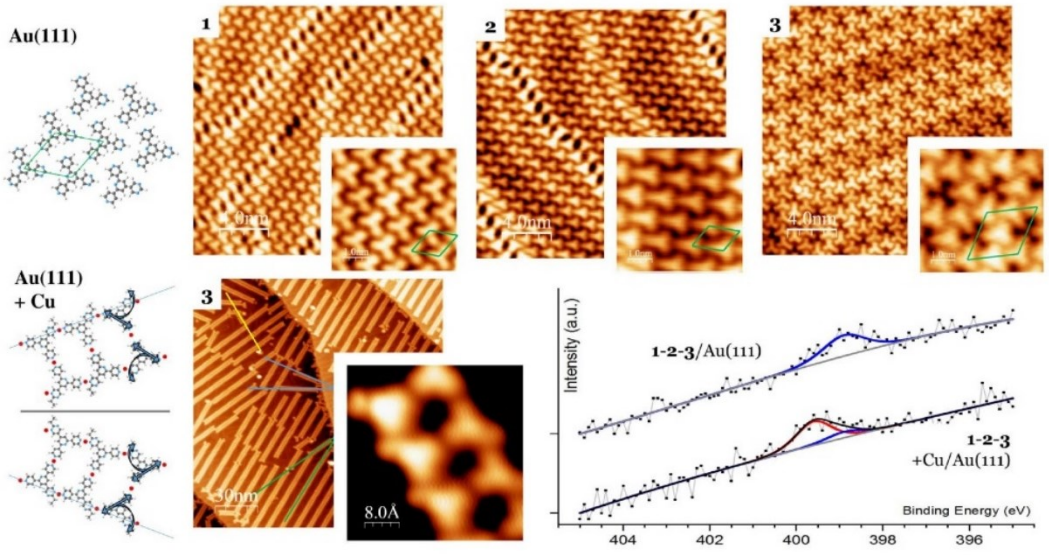

Fig. S8. Enlargement of manuscript Fig. 4.

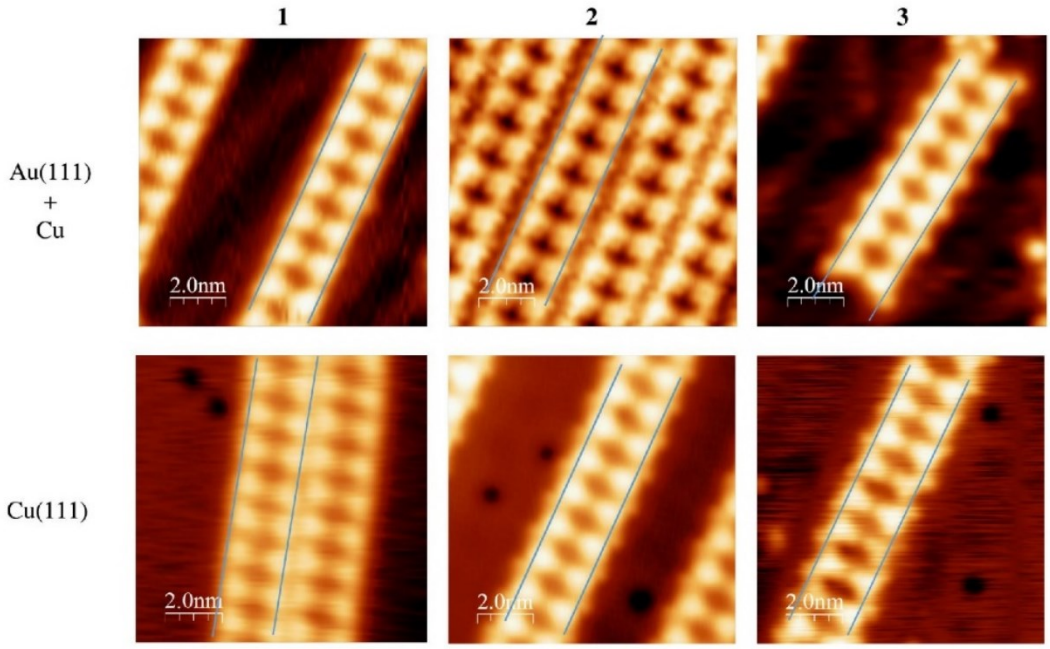

Fig. S9. The remarkable similarity between the chains of **1**, **2** and **3** on a) Au(111) + Cu adatoms (top row), b) Cu(111) (bottom row), and c) the chains of same compound on the different substrate (respective columns) is illustrated by drawing two parallel blue lines of 2.3 nm distance on all images, corresponding to the width of all ladders. Ethyl and methyl imaging groups are clearly seen on the outside of the blue lines. Please note: coverage of **2** on Au(111) was high; still chains are separated by a gap due to presence of the functionalization disabling proper stacking. In its absence however, e.g. in case of **1** on Cu, chains always make contact. On Au(111) the herringbone reconstruction is always visible on the substrate terraces; on Cu(111) "etching" spots are always visible.

S10

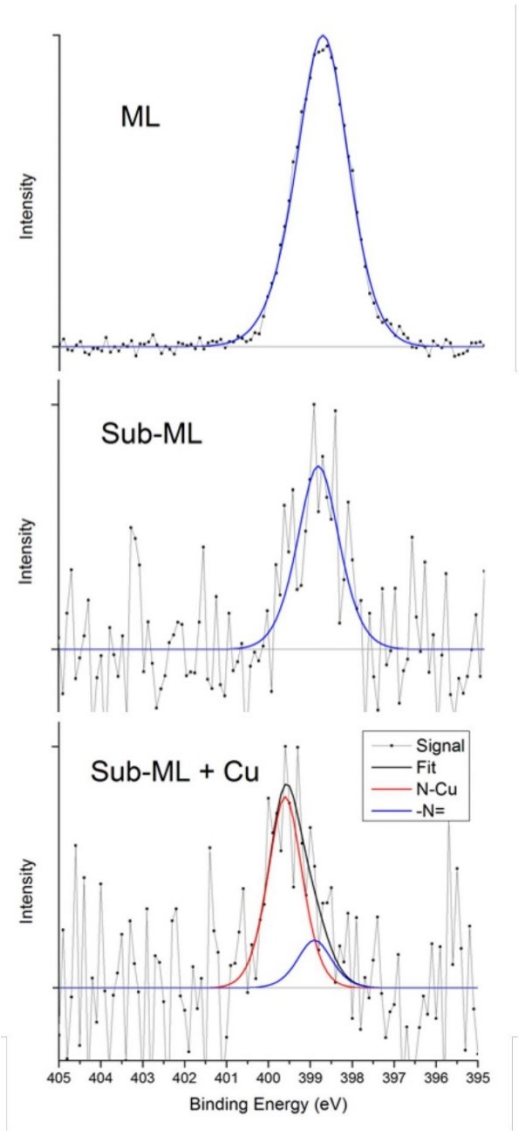

Fig. S10. Detailed N 1s peak analysis upon Cu-coordination of compound **1** (representative for all compounds) on Au(111) shows no peak position shift between multilayer and sub-mololayer coverages (probably due to little surface interaction; 398.8 eV). Upon Cu adatom supply at RT, coordination occurs at the four outer nitrogen atoms (new red peak; 399.6 eV). As previously reported, the central tpy nitrogen remains non-coordinated (remaining blue peak)[9], resulting in 4:1 ratio.

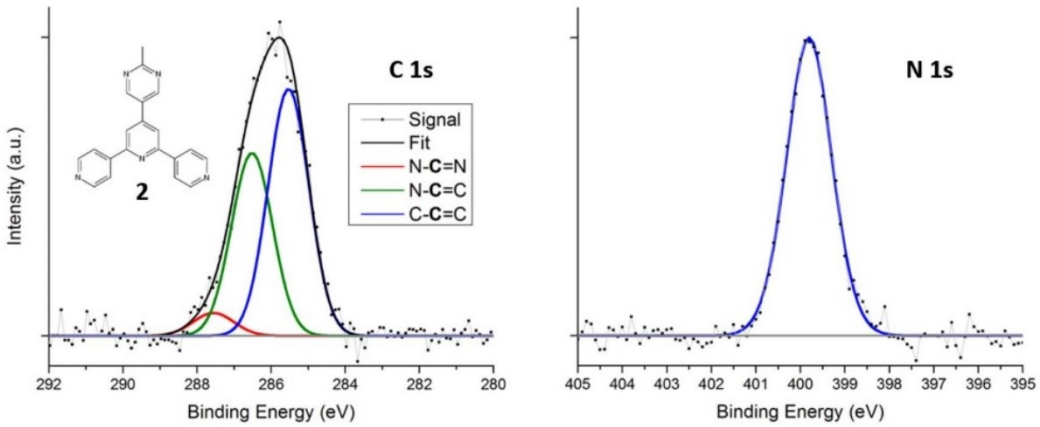

Fig. S11. XPS analysis of multilayer of **1, 2, 3** on Cu(111) presents similar results as on Au(111). Deconvolution of C 1s peak show correct C:C:C ratios, and all three compounds exhibit same N 1s peak. This is however situated at 399.8 eV. Also, C:N ratio changed from 4:1 to 5:1.

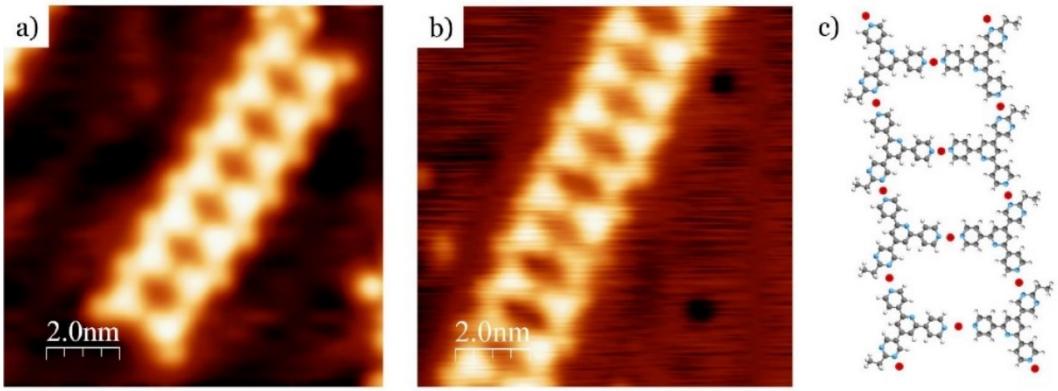

Fig. S12. Enlargement of manuscript Fig. 5.

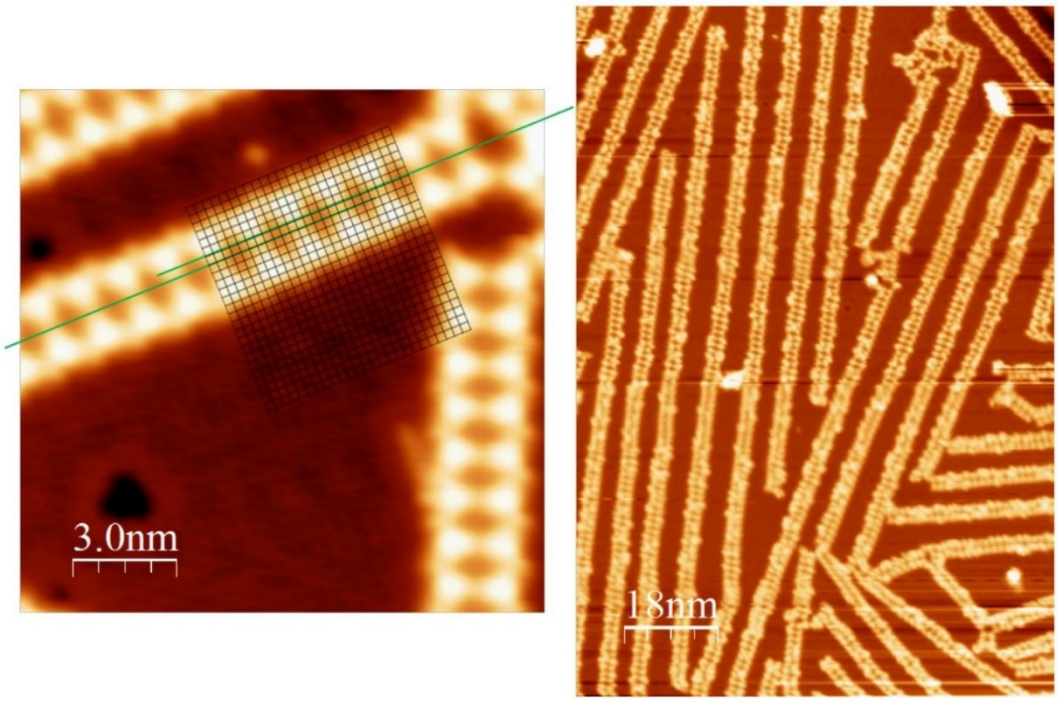

Fig. S13. Left: closer analysis of "wiggles" occurring in the chains. The two green lines are adjusted to the straight parts of the chains (middle nodal point as reference). Op top a 25x25 grid for more precise measurement, where one box is adjusted to match the distance between the two green lines. This turns out to be 2.56 Å, exactly corresponding to one lattice jump in the Cu substrate. Right: Chains exceed 125 nm of length (please note the presence of Xenon adatoms). Both images were taken on Cu(111) substrate.

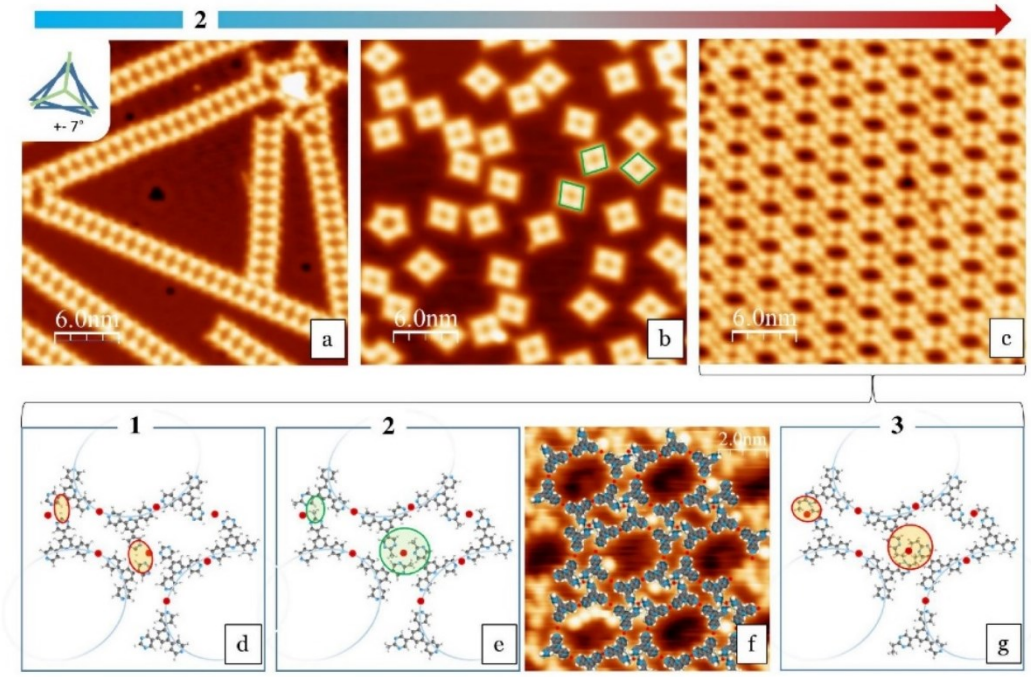

Fig. S14. Enlargement of manuscript Fig. 6.

S14

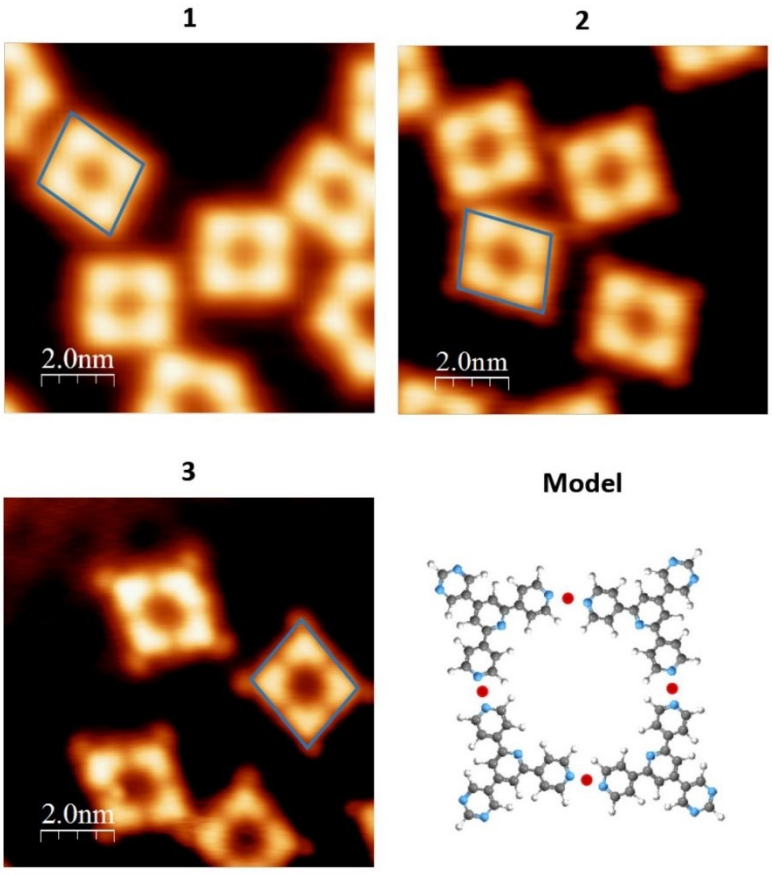

Fig. S15. Same blue rhombus of approx. 2.3 nm is drawn on top of tetramers of **1**, **2** and **3** on Cu(111). The as imaging groups acting methyl and ethyl functionalizations are clearly visible in the outside corners of the rhombuses, leaving the core unaltered for all three compounds.

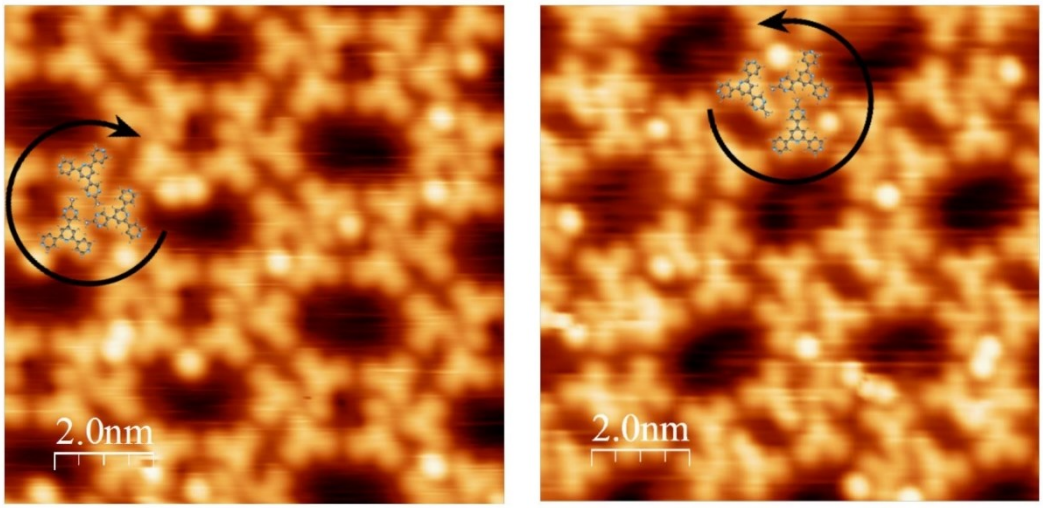

Fig. S16. The nanoporous assembly of **2** on Cu(111) is present in both chiralities.

S16

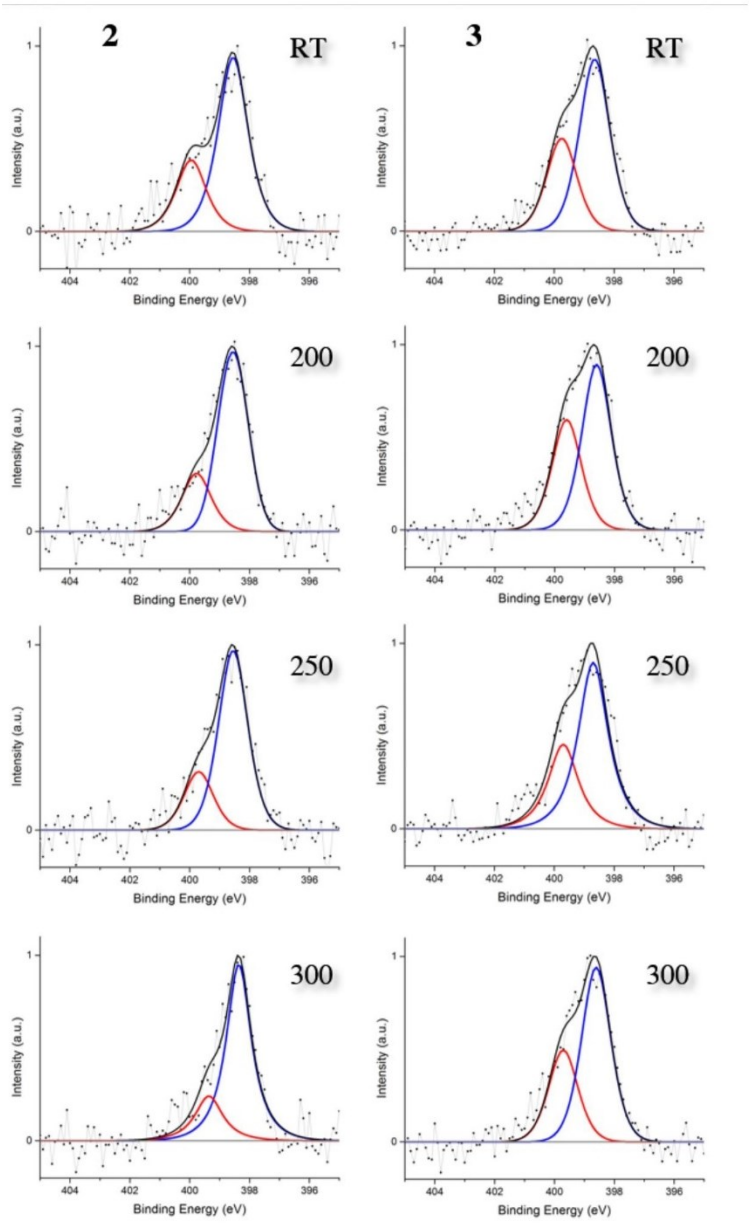

Fig. S17. Temperature dependent XPS analysis of **2** (left column) shows no difference, neither during annealing, nor between the different compounds (**3** in right column). Peak positions are 398.6 and 399.7 (± 0.2) eV in all cases.

S17

Table S1: XPS N 1s peak positions of **1,2,3** experimentally obtained:

Molecule/Substrate	**-N=** [eV]	**N-Cu** [eV]	
Multilayer **1,2,3**/Au(111)	398.8	-	
1,2,3/Au(111)	398.8	-	
1,2,3+Cu/Au(111)	398.8	399.6	
Multilayer **1,2,3**/Cu(111)	399.8	-	
1,2,3/Cu(111)	398.6	398.6	399.7
1,2,3/Cu(111) + Anneal	398.6	398.6	399.7

Table S2: Literature comparison of values in Table S1.

Molecule/Substrate	**-N=** [eV]	**N-Cu** [eV]
Multilayer **1,2,3**/Au(111)	398.9[9]	-
1,2,3+Cu/Au(111)	398,3[9,10,11] 398.5[12]	400.2[10] (Pt) 399.2[12] (Co) 399.7[9] (Cu)
Multilayer **1,2,3**/Cu(111)	399.1[13,14]	-
1,2,3/Cu(111)	397.8[15] 398.3[13,14] 398.8[17]	398.2[16] 398.2[14] 398.9[17]

Au(111):

- Similar peak position for multilayer as sub-monolayer as a result of no strong interaction of the compounds with the substrate.
- Major N 1s peak shift to higher binding energies upon coordination.[9,10,12]

Cu(111):

- Due to extra-atomic relaxation effect, multilayer N 1s peak is positioned at a higher binding energy than sub-monolayer N 1s peak.[13,14,18]
- Upon coordination, no major peak position change has been detected between non-coordinated and coordinated pyridylic N.[14,17]
- The second prominent and independent peak at higher binding energy cannot be neglected nor attributed to the shakeup process explained in references 11 and 12. Neither does it represent the coordinated nitrogen atoms -- we have reported examples of such non-fitting intra-atomic peak ratios in the past, especially of N 1s on Cu substrates,[19] but not to this extend; also is our current result in accordance to literature. The solution seems to lie in the nature of pyrimidine on Cu(111) surface, since the N 1s peak of 1,3,8,10-tetraazaperopyrene also exhibits an unexplainable additional peak on the higher binding energy, looking very similar to the result presented here (Figure B.3 in ref 15).

1. Klein, Y.M.; Constable, E.C.; Housecroft, C.E.; Zampese, J.A. *Polyhedron* **2014**, *81*, 98.
2 Stoe & Cie 2011; X-area Software. Stoe & Cie 1996; XRED V1.08.
3 Palatinus, L.; Chapuis, G. *J. Appl. Cryst.* **2007**, *40*, 786.
4 Betteridge, P.W.; Carruthers, J.R.; Cooper, R.I.; Prout, K.; Watkin, D.J. J. Appl. Cryst. **2003**, *36*, 1487.
5 Bruno, I.J.; Cole, J.C. ; Edgington, P.R.; Kessler, M.K.; Macrae, C.F.; McCabe, P.; Pearson, J.; Taylor, R. *Acta Cryst. B* **2002**, 58, 389.
6 Macrae, C.F.; Bruno, I.J.; Chisholm, J.A.; Edgington, P.R.; McCabe, P.; Pidcock, E.; Rodriguez-Monge, L.; Taylor, R.; van de Streek, J.; Wood, P.A. *J. Appl. Cryst.* **2008**, *41*, 466.
7 Blatov, V.A.; Shevchenko, A.P.; TOPOS Professional v. 4.0, Samara State University, Russia.
8 Horcas, I.; Fernandez, R.; Gomez-Rodriguez, J.M.; Colchero, J.; Gomez-Herrero, J.; Baro, A.M. *Rev. Sci. Instrum.* **2007**, *78*, 013705.
9 Nijs, T; Malzner, F.J.; Fatayer, S.; Wäckerlin, A.; Nowakowska, S.; Constable, E.C; Housecroft, C.E.; Jung, T.A *Chem. Commun.* **2015**, *51*, 12297.
10 Skomski, D.; Tempas, C.D.; Smith, K.A.; Tait, S.L *J. Am. Chem. Soc.* **2014**, *136*, 9861.
11 Li, Y.; Xiao, J.; Shubina, T.E.; Chen, M.; Shi, Z.; Schmid, M.; Steinrück, H.P.; Gottfried, J.M.; Lin, N. *J. Am. Chem. Soc.* **2012**, *134*, 6401.
12 Mette, G.; Sutter, D.; Gurdal, Y.; Schnidrig, S.; Probst, B.; Iannuzzi, M.; Hutter, J.; Albertob, R.; Osterwalder, J. *Nanoscale* **2016**, *8*, 7958.
13 Lin, Y.P.; Ourdjini, O.; Giovanelli, L.; Clair, S.; Faury, T.; Ksari, Y.; Themlin, J.M.; Porte L.; Abel, M. *J. Phys. Chem. C* **2013**, *117*, 9895.
14 Klappenberger, F.;. Weber-Bargioni, A.; Auwärter, W.; Marschall, M.; Schiffrin, A.; Barth, J.V. *J. Chem. Phys.* **2008**, *129*, 214702.
15 Matena, M.; Observing cooperative behavior with molecular surface structures, Dissertation, University of Basel 2009.
16 Matena, M.; Riehm, T.; Stöhr, M.; Jung, T.A. Gade, L.H.; Angew. Chem. Int. Ed. **2008**, *47*, 2414.
17 Li, J.; Wäckerlin, C.; Schnidrig, S.; Joliat, E.; Alberto, E.; Ernst, K.H. Helv. Chim. Acta **2017**, *100*, e1600278.
18 Kohiki, S.; Oki, K., Konishi, F. *Anal. Sci.* **1985**, *1*, 115
19 Shchyrba, A.; Wäckerlin, C.; Nowakowski, J.; Nowakowska, S.; Björk, J.; Fatayer, S.; Girovsky, J.; Nijs, T.; Martens, S.C.; Kleibert, A.; Stöhr, M.; Ballav, N.; Jung, T.A.; Gade, L.H. *J. Am. Chem. Soc.* **2014**, *136*, 9355.

Chapter [[3]]

Hierarchical chirality transfer of DiOH[6]Helicene on the self-assembly pattern: interplay of the complex intermolecular bonding

Summary:

This research focuses on the *in-situ* multi-stage chirality transfer from single helical molecules, over coordinated trimer to bigger supramolecular assemblies. *P*- and *M*- DiOH[6]Helicene molecules were deposited in enantiopure and racemic mixtures on Ag(111) substrates. Thereby they arrange/sort in homo-chiral trimers, in accordance with their initial chirality. Upon coordination of these assemblies, bigger regular clusters of trimer-of-trimers appeared, exhibiting still homo-chirality specific to the single molecular orientation, even after having switched the bonding motif. On the other hand, this allows for easy identification of the chirality of the single molecule by analysis of the bigger self-assembly.

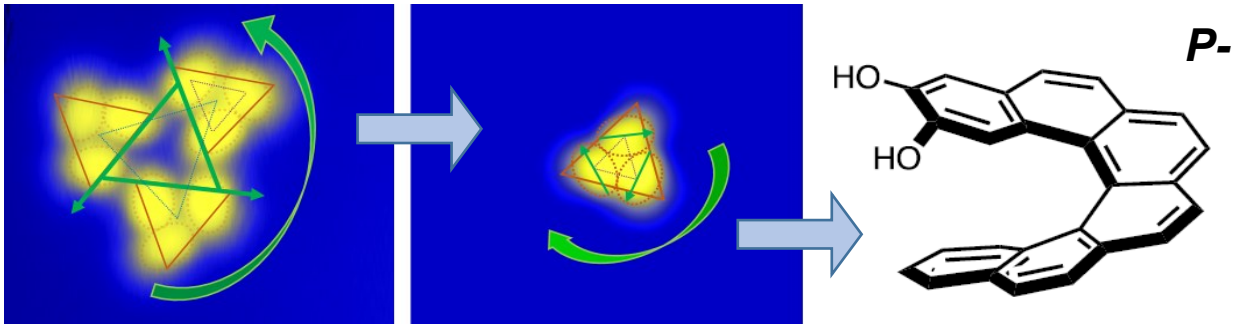

Contribution of T. Nijs: carried out the experimental investigation (STM, XPS), analysed and interpreted the data, wrote the manuscript. Synthesis part by D. Schweinfurth.

Hierarchical chirality transfer of DiOH[6]Hel on the self-assembly pattern: interplay of the complex intermolecular bonding

T. Nijs *et al.*

Motivation:

- Importance of chirality. Chirality transfer from single building block on supramolecular assembly at low molecular coverages is known to be strongly influenced by the flexibility of the molecule and strength of the intermolecular bonds.[1] Strong intermolecular bonding of functionalized helicenes at surfaces[1] in general, as well as particularly hydroxyl-functional groups reaction with transition metal adatoms are not well explored. Hierarchy of bonds and its influence on the assembly is not known for big chiral aromatic systems, as helicenes.
- We employ enantiopure catechol dihydroxy-functionalized *P* & *M*-hexahelicene (**diOH[6]Hel**) to investigate the impact of the complex intermolecular interactions/bonds on a supramolecular assembly and transfer of chirality.

Experimental results:

- X-ray photoelectron spectroscopy (XPS) study of the multilayer film (stoichiometry) evidences a proper sublimation of the molecule. Presence of the Ag(111) surface, however initiates a partial dehydrogenation of the molecules at sub-ML coverage, as was also shown in literature for carboxylic acids at Ag(111)[2,3], rendering **diOH[6]Hel** into **OOH[6]Hel.** The final molecular assembly is expected to be hydrogen-bonded.
- Adding of Co adatoms renders the initial 2 peaks of O1s into 1 peak with a chemical shift in O1s XPS signal of 2.5 eV with respect to the multilayer film, indicating a full dehydrogenation of hydroxyl-groups and formation of coordination complex with Co, **Co(OO[6]Hel)$_3$**.
- Switch of the bonding motif from H-bonding to metal coordination switches the self-assembly.
- Self-assembly on Au(111) was difficult to detect by scanning tunneling microscope (STM) due to its instability – provides however useful information.

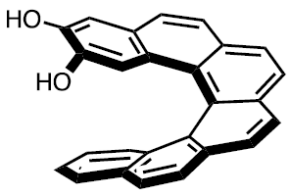

Figure 1 Synthesis part by David Schweinfurth.

We probe the chemical state of the on-surface adsorbed **diOH[6]Hel** by the element specific XPS measurements of the O1s core level shifts (Figure 2). XP spectrum of the multilayer shows a single O1s peak 533.4 eV, reflecting the same chemical environment of hydroxyl groups[4,5,6,7] (green, Figure 2). The width of the peak is slightly bigger, as one would expect on the basis of resolution (1 eV FWHM), and reaches 1.4 eV FWHM due to intermolecular hydrogen bonds[2]. At submonolayer coverage the O1s spectra contain two peaks, first peak at 532.7 eV corresponding to *hydroxyl*-group[2,3,5] (green) and the second peak at 530.8 eV corresponds to *ketone*-group[2,3,5,6] (red). Appearance of the second peak evidences a partial dehydrogenation of the molecule to **OOH[6]Hel** in the sub-ML case promoted by the direct contact with the substrate[2,4,8]. Upon Co-adatom supply, a single O1s peak is observed at 530.9 eV. Thus the molecule is completely dehydrogenated and metal coordinated **Co(OO[6]Hel)$_3$**. All the XPS peaks positions and comparison with the literature values are summarised in Table 1.

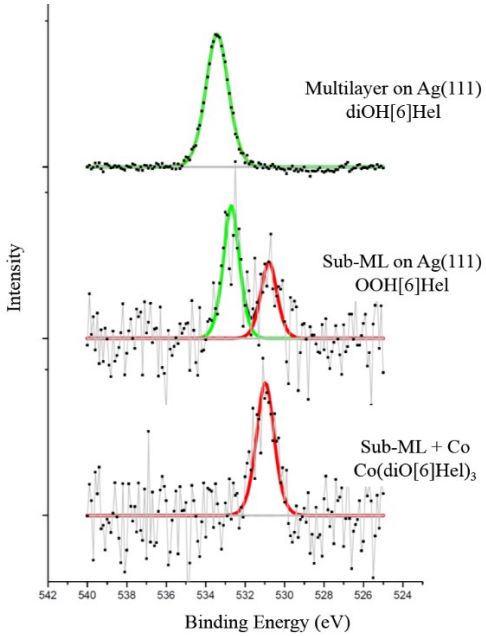

Sample	Literature	Experiment
Hydroxyl		
Multilayer	533.5[4] / 533.6[5,6] / 533.8[7]	**533.4**
Sub-ML	532.6[3,5] / 532.8[2]	**532.7**
Ketone		
Sub-ML	530.3[2] / 530.9[3] / 531.2[6] /531.4[5]	**530.8**
Sub-ML + Co	-	**530.9**

Table 1 Summarizing comparison of experimental XPS O1s peak positions to literature values.

Figure 2 XPS of O1s core level analysis for multilayer diOH[6]Hel, sub-monolayer and sub-monolayer in the presence of Co adatoms. Green curve reflects the hydroxyl-group and red curve keton-group. See main text for more details.

STM images (all images taken with typical tunneling parameters, 6 pA, +- 500 mV) of enantiopure ***(P)*-diOH[6]Hel** in submonolayer coverage on Ag(111) substrate show a trimeric arrangement. Single trimers are consisting of three hydrogen bonded molecules (Fig. 2c) and are distributed on the distance from each other reflecting rather repulsive interactions. At closer look, molecules appear in STM images slightly elongated and oval shaped, resulting in homochiral trimers, as highlighted in Fig 3b.

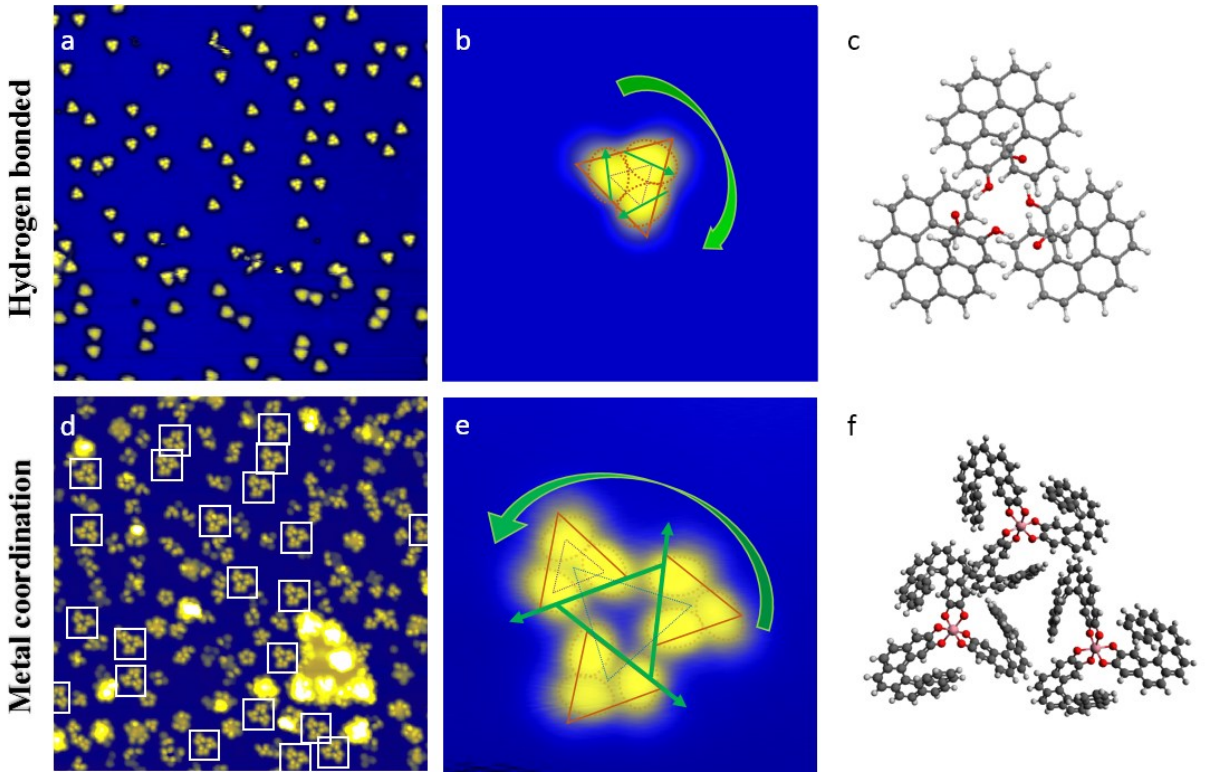

Figure 3 Self-assembly of (P)-diOH[6]Hel on Ag(111) depends on the type of the intermolecular interactions. (a) Deposition of diOH[6]Hel on Ag(111) at RT renders partial dehydrogenation and results in H-bonded structures OOH[6]Hel; Overview of the assembly (50 x 50 nm^2). (b) Single trimer has a chiral orientation, marked by green arrow (5 x 5 nm^2). (c) Molecular model of the intermolecular H-bonding arrangement. (d) Adding of Co-adatoms promotes dehydrogenation of OOH[6]Hel into OO[6]Hel and formation of metal coordinated complex $Co(OO[6]Hel)_3$. Upon subsequent annealing, triple-trimers are dominating the assembly (50 x 50 nm^2). (e) Chirality transfer from single trimers towards the triple-trimer (5 x 5 nm^2). (f) Molecular model of the intermolecular arrangement with complex intermolecular interactions: metal coordination and vdW forces.

After addition of Co adatoms and subsequent annealing of the very same sample, the dominating assembly is changed from trimers to 'trimer of trimers'. In XPS we observe a chemical modification of molecule, i.e. full dehydrogenation and metal coordination. The dimensions of the single trimers are also increased with the switch of the bonding motif: regular a = b = c = 0.58 nm vs. a = 0.56 nm, b = 0.68 nm, c = 0.71 nm (centre of molecule to centre of molecule according to dotted purple line), for H-bond vs metal coordination, respectively, and 1.5 nm in-between the trimers of **$Co(OO[6]Hel)_3$** (dotted blue line). The resulting metal coordinated trimers are attracted by vdW interactions (to be checked), demonstrating an interesting interplay of strong metal-coordination beside weak attractive forces (see model, Fig. 2c). Being helical and flexible,[1] helicene molecules are able to bind to a central Co-adatom from all sides, resulting in octahedral configuration (6 binding sites: 2 sites for each molecule). This octahedral binding configuration is thereby yielding the overall chirality of the single trimers. The chirality of the contained single trimmers is the same as in the hydrogen bonded case, however, the overall chirality of the assembly is in the opposite directions.

Hydrogen bonded samples are not exclusively covered with trimers, as depicted in Fig. 4a, but consist on average by 10% of tetrameric assemblies as well (see Fig. 4b). These tetramers are same loosely bound (see SI as how easily both assemblies can be modified by STM tip), and express interestingly the same chirality as the same enantiopure trimers.

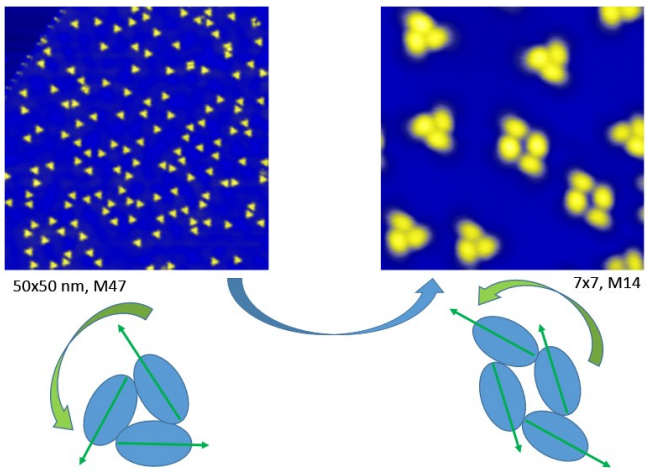

Figure 4 Samples are predominantly, but not exclusively covered with trimers. A small amount of tetramers is present in co-existence, --- the same.

As shown so far, deposition of enantiopure (P)-diOH[6]Hel on Ag(111) results exclusively into clockwise oriented chiral hydrogen bonded assemblies, whereas the resulting Co-coordinated super trimers are exclusively in anticlockwise chirality. This behavior is exactly reproducible in the similar reversed way for enantiopure (M)-diOH[6]Hel, where the hydrogen bonded assemblies are exclusively anticlockwise and the coordinated assemblies exclusively clockwise oriented.

Upon racemic mixture of both types, molecules show narcissistic behavior. Fig 5a displays two trimers of hydrogen bonded OOH[6]Hel/Ag(111), one bearing clockwise, the other anticlockwise chirality. This shown both handednesses of molecules don't intermix. Same separation is also seen in the coordinated case, where again both conformations coexist.

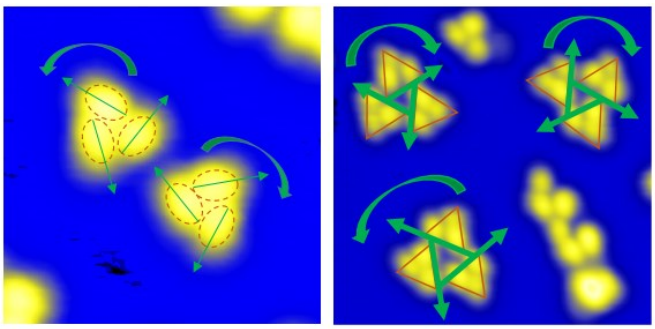

Figure 5 Racemic mixtures sort in their enantiopure assemblies, in both a) the hydrogen bounded case, and b) the coordinated case.

1. Shchyrba, A. *et al.* Chirality Transfer in 1D Self-Assemblies: Influence of H-Bonding vs Metal Coordination between Dicyano[7]helicene Enantiomers. *J. Am. Chem. Soc.* **135,** 15270–15273 (2013).
2. Giovanelli, L. *et al.* Combined Photoemission Spectroscopy and Scanning Tunneling Microscopy Study of the Sequential Dehydrogenation of Hexahydroxytriphenylene on Ag(111). *J. Phys. Chem. C* **118,** 14899–14904 (2014).
3. Schnadt, J. *et al.* Interplay of adsorbate-adsorbate and adsorbate-substrate interactions in self-assembled molecular surface nanostructures. *Nano Res.* **3,** 459–471 (2010).
4. Fischer, S. *et al.* L-Cysteine on Ag(111): A Combined STM and X-ray Spectroscopy Study of Anchorage and Deprotonation. *J. Phys. Chem. C* **116,** 20356–20362 (2012).
5. Li, H., Xu, B., Evans, D. & Reutt-Robey, J. E. Isonicotinic Acid Molecular Films on Ag(111): I. XPS and STM Studies of Orientational Domains. *J. Phys. Chem. C* **111,** 2102–2106 (2007).
6. Schiffrin, A. *et al.* Zwitterionic self-assembly of L-methionine nanogratings on the Ag(111) surface. *Proc. Natl. Acad. Sci.* **104,** 5279–5284 (2007).
7. Stepanow, S. *et al.* Deprotonation-Driven Phase Transformations in Terephthalic Acid Self-Assembly on Cu(100). *J. Phys. Chem. B* **108,** 19392–19397 (2004).
8. Fischer, S. *et al.* Self-Assembly and Chemical Modifications of Bisphenol A on Cu(111): Interplay Between Ordering and Thermally Activated Stepwise Deprotonation. *ACS Nano* **8,** 207–215 (2014).

Conclusion

During this thesis, we wanted to explore to which extent the investigation of complex 3D assemblies, and hierarchical 2D assemblies, can be facilitated by breaking down their dimensionality. To do so, we present the unique approach of employing the very same molecules in a direct on-surface vs. in-solution comparison. Are we still able to draw conclusions if we investigate the simplified 2D self-assembly and are we able to extrapolate this result to 3D? Will the substrate, introduced as dimension-reducing agent, be a curse of a blessing?

To tackle these questions, a new terpyridine molecule has been designed, allowing for planar 2D spreading by use of its divergent positioning of the N atoms -- in contrast to the usual chelating 2,2':6',2"-terpyridine. In a first experiment, the first self-assembly investigation of such functionalized 4,2':6',4"-terpyridines at the solid-vacuum interphase is presented. Thereby we reveal the availability of additional coordination sites as compared to the in-solution case. Additionally, the influence of the substrate, non-existing in solution experiments, has been shown by changing the bonding motif from hydrogen bonded to metal coordinated. Thereby the molecules are pulled down towards the surface, and orient along the herringbone surface reconstruction on Au(111).

In a second experiment, we report deeper understanding of tuning of the on-surface assembly of 4,2':6',4"-terpyridines, by either changing the functionalization or by applying external stimuli. Even smallest changes of the molecules lead to drastic assembly changes, as well as titration of Cu adatoms provided from the substrate by heat. This is compared to 3D X-ray crystallographic data where assembly changes are mostly related to the used Cu-salts and the way these bridge neighboring molecules including the influence of the counterions and solvents. This greatly drives the geometry of the connecting nodes and the interactions between the 2D sheets.

The last chapter follows the same principle, but in another concept. This time we investigate the 2D hierarchical growth of complexes, from the single building block. More precisely, we track the propagation of chirality upon different changes of the self-assembly. Due to its great flexibility, helicene molecules are predestinated for these experiments. With proper choice of functionalization they allow for both, hydrogen bonding and metal coordination, as well as a coordination-van der Waals mixed assembly, each preserving a well-defined handedness, determined by the individual molecules.

In conclusion, in the case of the 2D on-surface chirality transfer we are able to directly relate the handedness of the multi-stage processed assembly to the individual building block molecule, even including all intermediate steps. While changing the medium from vacuum to in-solution however, the assembly-guiding parameters also change significantly. Having some specific rules being true for both cases, in-solution and at the solid-vacuum interphase (like $NH_{imidazole} \cdots N_{tpy}$ hydrogen bonding outperforming $NH_{imidazole} \cdots N_{imidazole}$), others differ quite significantly (like the presence of additional coordination sites on-surface, giving rise to new assembly possibilities). Furthermore, even though the usage of the very same molecules and the presence of 2D sheets in all cases, the strong fixation of the metal coordination nodes to the metal substrate vs. the 3D freedom of solvents and counterions significantly alters the self-assembly.

Acknowledgements

My main thanks go to my PhD supervisors Catherine Housecroft and Thomas Jung for having shaped the outlines for such a great project. I would choose the same project again!

Many thanks also go to all the people I worked together with during these four years:

To start with, the crew of Nanolab, from my senior colleagues Toni Ivas, Aneliia Wäckerlin (née Shchyrba) and Sylwia Nowakowska for letting me learn so much, to the current members, especially Aisha Ahsan with whom I basically have spent my entire PhD together, and S. Fatemeh Mousavi for having shared with me such an incredible amount of lab time. Not to forget technical support (there especially Marco Martina, for being such a great lad!).

Then many thanks go to the Housecroft/Constable research group, with whom it was great fun to work together with, to have team meetings with and to plan towards a successful collaboration. Especially Maximilian Klein and Frederik Malzner are to be mentioned here.

In the same breath I also want to thank my external collaborators from ETH, in the first place François Diederich, Carlo Thilgen and Jovana Milic.

From LMN at PSI: Both Jan's especially (Girovski and Nowakowski) for the introduction and help with spectroscopy experiments, seniors Christian Wäckerlin, Harald Rossmann and Dorota Siewert for amazing times there, and all the new people. Again separate acknowledgement for technical support by Rolf Schelldorfer.

Thanks also go to the Nanolino guys next door, and maybe even most importantly to all people in the background, who did an at least same important job.

Last but not least I want to mention all blockcourse-, project-, seminar-, summer-, exchange- and master-students which I supervised or worked with. In alphabetic order these were: Laurent Clarissou, Shadi Fatayer, Philipp Gigler, Mac Iwasaki, Bianca Leykam, Anna Morales, Mariah O'Doherty, Timo Philipp, Till Ryser, Matej Siketanc, Robert Skonieczny, Daniel Stähli, Alexis Tello and Marco Zutter. It's always fun to teach and work with the next generation!

I am grateful for all people who were around during this time and contributing to make it a great and unforgettable time.

Bibliography

1 Marc J. Madou, Fundamentals of microfabrication: the science of miniaturization, 2nd Ed., *CRC Press*, 2002

2 Paul S. Peercy, The drive to miniaturization, *Nature*, **406**, 1023-1026 (2000)

3 G.E. Moore, Cramming More Components Onto Integrated Circuits, *Electronics*, 114–117 (1965)

4 Rachel Courtland, Intel Hits Snag On The Way To Next-Generation Chips, *IEEE Spectrum* (2015) http://spectrum.ieee.org/tech-talk/semiconductors/devices/intel-hits-snag-on-way-to-nextgeneration-chips

5 Chris Mack, The Multiple Lives of Moore's Law, *IEEE Spectrum* (2015) http://spectrum.ieee.org/semiconductors/processors/the-multiple-lives-of-moores-law

6 M. Mitchell Waldrop, The chips are down for Moore's law, *Nature*, **530**, 144-147 (2016)

7 Bart Kolodziejczyk, The 5 next trends in electronics, *World Economic Forum* (2015) https://www.weforum.org/agenda/2015/08/5-next-trends-in-electronics/

8 Martin Fuechsle, Jill A. Miwa, Suddhasatta Mahapatra, Hoon Ryu, Sunhee Lee, Oliver Warschkow, Lloyd C.L. Hollenberg, Gerhard Klimeck & Michelle Y. Simmons, A single-atom transistor, *Nature Nanotechnology*, **7**, 242–246 (2012)

9 Philip Skehan, Ritsa Storeng, Dominic Scudiero, Anne Monks, James McMahon, David Vistica, Jonathan T. Warren, Heidi Bokesch, Susan Kenney, Michael R. Boyd, New Colorimetric Cytotoxicity Assay for Anticancer-Drug Screening, *JNCI*, **82**, 1107–1112 (1990)

10 Bo Zheng, L. Spencer Roach, and Rustem F. Ismagilov, Screening of Protein Crystallization Conditions on a Microfluidic Chip Using Nanoliter-Size Droplets, *J. Am. Chem. Soc.*, **125**, 11170–11171 (2003)

11 David Lee, Oliver Redfern & Christine Orengo, Predicting protein function from sequence and structure, *Nature Reviews Molecular Cell Biology*, **8**, 995-1005 (2007)